



# Sulfated glycans engage the Ang-Tie pathway to regulate vascular development

Matthew E. Griffin<sup>1</sup>, Alexander W. Sorum<sup>1</sup>, Gregory M. Miller<sup>1</sup>, William A. Goddard III<sup>1</sup>, and Linda C. Hsieh-Wilson<sup>1</sup>

The angiopoietin (Ang)-Tie pathway is essential for the proper maturation and remodeling of the vasculature. Despite its importance in disease, the mechanisms that control signal transduction through this pathway are poorly understood. Here, we demonstrate that heparan sulfate glycosaminoglycans (HS GAGs) regulate Ang-Tie signaling through direct interactions with both Ang ligands and Tie1 receptors. HS GAGs formed ternary complexes with Ang1 or Ang4 and Tie2 receptors, resulting in potentiation of endothelial survival signaling. In addition, HS GAGs served as ligands for the orphan receptor Tie1. The HS-Tie1 interaction promoted Tie1-Tie2 heterodimerization and enhanced Tie1 stability within the mature vasculature. Loss of HS-Tie1 binding using CRISPR-Cas9-mediated mutagenesis in vivo led to decreased Tie protein levels, pathway suppression and aberrant retinal vascularization. Together, these results reveal that sulfated glycans use dual mechanisms to regulate Ang-Tie signaling and are important for the development and maintenance of the vasculature.

ascular tissue changes dynamically over the lifespan of an organism in response to development, growth and injury<sup>1,2</sup>. The balance between vessel formation, stabilization and regression is coordinated by numerous signaling molecules at the surface of endothelial cells<sup>3</sup>. During angiogenesis, endothelial cells are regulated by several receptor tyrosine kinase (RTK) pathways, including the vascular endothelial growth factor receptor (VEGFR)<sup>4</sup>, fibroblast growth factor receptor (FGFR)<sup>5</sup> and platelet-derived growth factor receptor (PDGFR) pathways<sup>6</sup>, via the spatiotemporally controlled expression and release of ligands from the surrounding tissue. Mechanisms to coordinate the assembly and activation of ligand–receptor complexes at the cell surface are thus vital for the proper growth, patterning and maturation of blood and lymphatic vessels.

Many of these ligands and receptors bind to linear, sulfated polysaccharides known as GAGs, which are anchored to the cell surface or secreted into the extracellular matrix<sup>7,8</sup>. Interactions between GAGs and proteins modulate signal transduction in various important biological contexts, such as cell differentiation<sup>9</sup>, tissue formation<sup>10</sup> and wound repair<sup>11</sup>. However, the structural complexity of GAG chains, which contain up to 100 disaccharide units and display diverse sulfation motifs<sup>7,8</sup>, has challenged efforts to identify and characterize GAG–protein interactions.

Numerous studies have revealed that HS GAGs are key regulators of vascular development. For example, genetic deletion of HS biosynthetic enzymes leads to severe vascular defects and edema, as well as embryonic or neonatal lethality in mice<sup>12,13</sup>. At the molecular level, HS GAGs facilitate the interactions of VEGF<sub>165</sub> and VEGFR2 and thereby promote cell proliferation, migration and endothelial tube formation<sup>4,14,15</sup>. HS GAGs are also implicated in the regulation of other angiogenic ligand–receptor complexes such as FGF2/FGFR1 (refs. <sup>5,16,17</sup>) and PDGF-BB/PDGFR<sup>18</sup>. While previous work has focused on HS GAGs during sprouting angiogenesis<sup>13,19</sup>, the functions of GAGs during blood vessel maturation and homeostasis have received far less attention. Therefore, we postulated that HS

GAGs might play additional roles in regulating the vascular system through as yet unidentified GAG-protein interactions.

The Ang-Tie RTK pathway is critical for the establishment and maintenance of both normal and disease-associated vasculature<sup>20,21</sup>. This endothelial signaling pathway is required for the maturation and pruning of blood and lymphatic vessels during development and their homeostasis during adulthood. In mammals, the pathway comprises two cell-surface receptors, Tie1 and Tie2, and three soluble ligands, Ang1, Ang2 and Ang4. Genetic deletion of either receptor results in embryonic or neonatal lethality in mice, and the resultant embryos exhibit severe edemic phenotypes<sup>22,23</sup>. Signaling in the Ang-Tie pathway is thought to occur exclusively via activation of Tie2 receptors. Ang1 or Ang4 ligands promote the oligomerization of Tie2, which leads to Tie2 cross-phosphorylation, stimulation of downstream Akt signaling and nuclear export of the transcription factor FOXO1 (Fig. 1a)20. In contrast, Ang2 acts as a context-dependent agonist or antagonist of Tie2 activity during vessel remodeling<sup>24</sup>. Aberrations in these signaling pathways contribute to tumor development, sepsis and diabetes-associated complications<sup>21</sup>. As such, numerous therapeutics targeting Ang1, Ang2 and Tie2 have entered clinical trials to treat a diverse range of diseases<sup>21</sup>.

Unlike Tie2, the Tie1 receptor is an orphan receptor<sup>25</sup> and its functions are much less well understood. Although early studies proposed that Tie1 inhibits Tie2 signaling<sup>26</sup>, recent evidence suggests that Tie1 acts in a context-dependent manner via transient interactions with Tie2 (refs. <sup>27,28</sup>). The formation of Tie1–Tie2 heterodimers has been suggested to prevent Tie2 activation and rapid internalization, which in turn maintains a population of Tie2 receptors at the cell surface and sustains Tie2 signaling (Fig. 1a)<sup>29,30</sup>. Interestingly, Tie1 was also recently linked to tumor progression and metastasis, wherein loss of Tie1 on endothelial cells decreased new vessel formation in primary tumors and reduced secondary lung metastases<sup>31,32</sup>. These studies implicate Tie1 as an anticancer target and further highlight the importance of obtaining a better mechanistic understanding of Ang–Tie pathway regulation.

<sup>1</sup>Division of Chemistry and Chemical Engineering, California Institute of Technology, Pasadena, CA, USA. <sup>2</sup>Materials and Process Simulation Center and Joint Center for Artificial Photosynthesis, California Institute of Technology, Pasadena, CA, USA. <sup>3</sup>These authors contributed equally: Alexander W. Sorum, Gregory M. Miller. <sup>™</sup>e-mail: lhw@caltech.edu

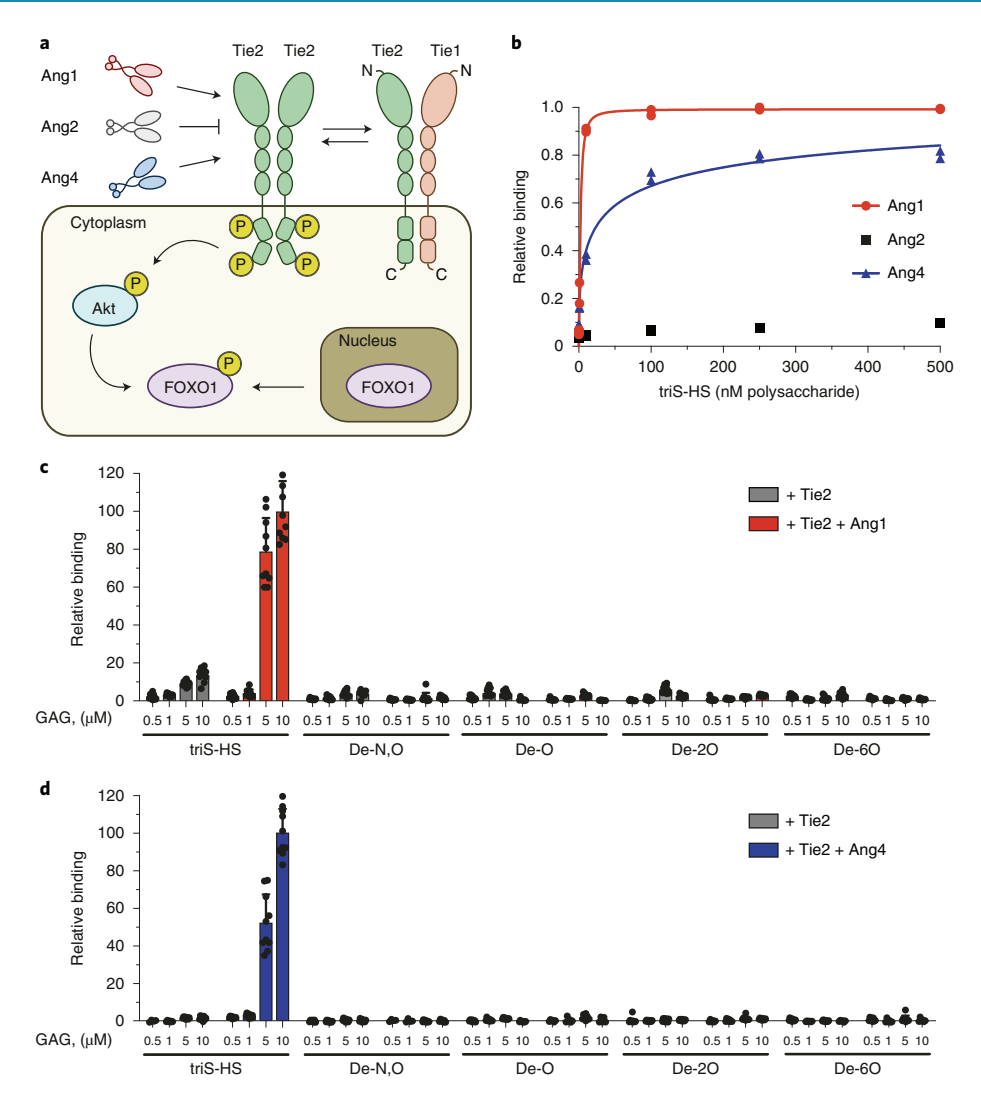


**Fig. 1** | **HS GAGs engage Ang1 and Ang4 ligands to form ternary complexes with Tie2. a**, Schematic of the Ang–Tie signaling pathway in which Ang ligands and Tie1 can act as agonists or antagonists of Tie2 phosphorylation and downstream signaling. N and C termini of the Tie proteins are indicated by N and C. **b**, ELISA-based detection of biotinylated triS-HS bound to immobilized Ang1, Ang2 and Ang4. Dissociation constants:  $K_{D,app}$  (Ang1): 2.23 nM (1.69 to 2.87 nM) and  $K_{D,app}$  (Ang4): 41.8 nM (9.73 nM to 21.0 μM). Values represent the mean (95% CI); graphed data represent n=2 independent replicates. **c,d**, Binding of Tie2-Fc ectodomain to a chemically defined HS GAG microarray in the presence or absence of Ang1 (**c**) or Ang4 (**d**). Data represent the mean ± s.e.m.; n=10 individual spots per glycan concentration.

Here, we report that HS GAGs play a key role in regulating the Ang–Tie RTK signaling axis. Through direct interactions with both Ang ligands and the orphan receptor Tie1, HS GAGs direct the assembly of cell-surface receptor complexes and modulate prosurvival signaling. Furthermore, loss of HS GAG regulation leads to decreased pathway activation and altered vascularization in vivo. Together, these results provide new insights into the molecular mechanisms that control Ang–Tie RTK signaling and suggest new roles for HS GAGs in the formation, maturation and homeostasis of complex vascular tissue.

#### Results

HS GAGs bind to angiopoietin ligands Ang1 and Ang4. As HS GAGs regulate other RTK pathways by interacting with soluble ligands<sup>8,13</sup>, we first examined whether HS GAGs bind to the angiopoietins Ang1, Ang2 and Ang4. A modified ELISA<sup>33</sup> was used to detect the binding of biotinylated HS GAGs to immobilized Ang

ligands. HS GAGs enriched in the N-, 2-O- and 6-O-sulfated HS motif (triS-HS) showed nanomolar affinity for Ang1 and Ang4 and no measurable affinity for the antagonist Ang2 (Fig. 1b). Interestingly, the observed binding preferences for anionic HS GAGs were not predicted based on the theoretical isoelectric (pI) values of the ligands (6.20 for Ang1, 5.34 for Ang2 and 8.65 for Ang4).

We next examined whether HS GAGs could form ternary complexes with Ang1 or Ang4 and the Tie2 receptor. For this, we used our GAG microarray platform, which was successfully used to detect HS-FGF-FGFR interactions<sup>34</sup>. Tie2 alone showed little affinity for any of the HS GAG structures on the microarray (Fig. 1c,d), as confirmed by ELISA (Extended Data Fig. 1). However, when Tie2 was added with Ang1 or Ang4, we observed robust localization of Tie2 to triS-HS on the microarray. These results suggest that Ang ligands recruited by the immobilized HS GAGs can interact with Tie2 and form ternary GAG-ligand-receptor complexes. Notably,

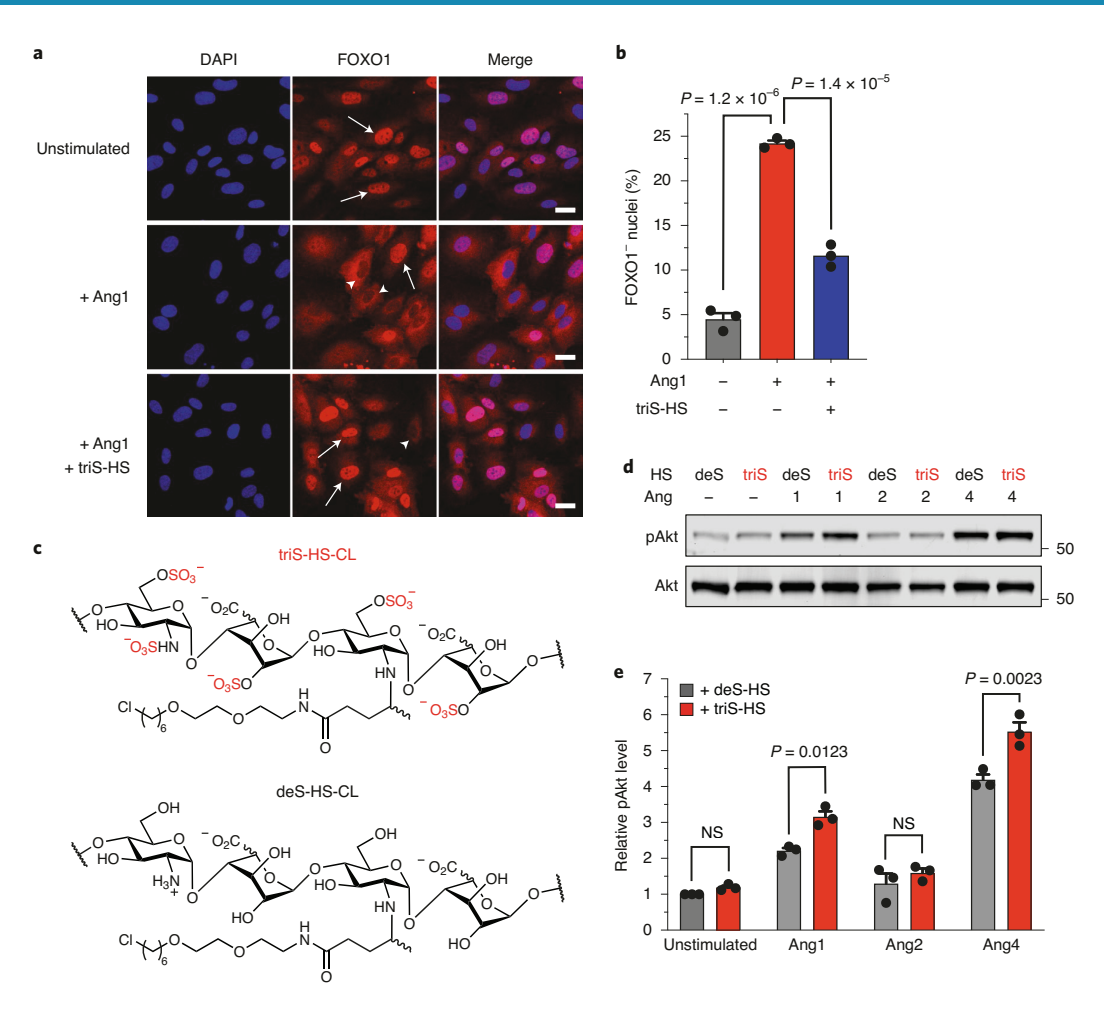


Fig. 2 | Ang-HS binding positively regulates prosurvival signaling. a,b, Representative images (a) and quantification (b) of FOXO1 export (red) from the nuclei (blue, DAPI) of HUVECs after stimulation with either Ang1 alone or Ang1 preincubated with excess triS-HS; arrows: FOXO1+ nuclei; arrowheads: FOXO1- nuclei; scale bar:  $50 \, \mu m$ . Data represent the mean  $\pm$  s.e.m.; n=3 biologically independent samples, one-way ANOVA with Tukey's post hoc test. **c**, Chemical structures of triS-HS and deS-HS conjugated to the chlorohexyl linker (CL) for cell-surface glycan engineering of HTP-expressing cells. **d**,**e**, Representative western blots (**d**) and quantification (**e**) of Akt phosphorylation in EA.hy926 cells engineered to display either triS-HS or deS-HS after stimulation with Ang1, Ang2 or Ang4. Phosphorylated-Akt values were normalized to the corresponding total Akt levels and are reported relative to unstimulated deS-HS. Data represent the mean  $\pm$  s.e.m.; n=3 biologically independent samples; two-way ANOVA with Sidak's multiple-comparisons test. NS, not significant.

complex formation was hindered by loss of HS sulfation, indicating that Ang1 or Ang4 binding to HS GAGs and ternary complex formation occurred in a sulfation-dependent manner.

Cell-surface triS-HS regulates prosurvival signaling. As triS-HS bound to agonists of Tie2 signaling, we hypothesized that HS GAGs may promote the formation of activated signaling complexes and positively regulate cell survival pathways. To test this, we stimulated human umbilical vein endothelial cells (HUVECs) with Ang1 and monitored the export of FOXO1 from the nucleus (Fig. 1a). Compared to unstimulated cells, we saw a significant increase in the number of FOXO1- nuclei (Fig. 2a,b), consistent with an increase in Ang1-dependent Tie2 signaling. Nuclear export of FOXO1 was significantly blocked by preincubation of Ang1 with an excess of soluble triS-HS, suggesting that Ang1 binding to cell-surface HS GAGs was competed away by soluble GAGs.

We next investigated whether Tie2 signaling was potentiated by directly remodeling HS GAGs on the cell surface. For this, we utilized our established glycan engineering method, whereby a

transmembrane HaloTag protein (HTP) is heterologously expressed on the cell surface<sup>35</sup>. Reaction of an aspartic acid residue in the HTP with a chloroalkyl group on functionalized GAGs forms a covalent linkage, enabling cell-surface display of desired GAG structures and mimicking the natural presentation of GAGs on proteoglycans (Supplementary Fig. 1a). We first produced a lentivirus to stably express the HTP on the surface of EA.hy926 human endothelial cells. HTP expression was confirmed by labeling the cells with Alexa Fluor 488 dye conjugated to a chlorohexyl linker (AF488-CL) (Supplementary Fig. 1b). We then treated the cells with chlorohexyl linker-modified triS-HS (triS-HS-CL)35 or chemically desulfated HS (deS-HS-CL; Fig. 2c) before stimulating the cells with different Ang ligands. Cells engineered to display triS-HS showed a marked increase in Akt phosphorylation compared to cells engineered with deS-HS upon stimulation with the Tie2 agonists Ang1 and Ang4, but not the Tie2 antagonist Ang2 (Fig. 2d,e). Together, these results demonstrate that HS GAGs can engage in ternary complexes with Ang1 or Ang4 and Tie2 and regulate downstream activation of the pathway.

**ARTICLES** 

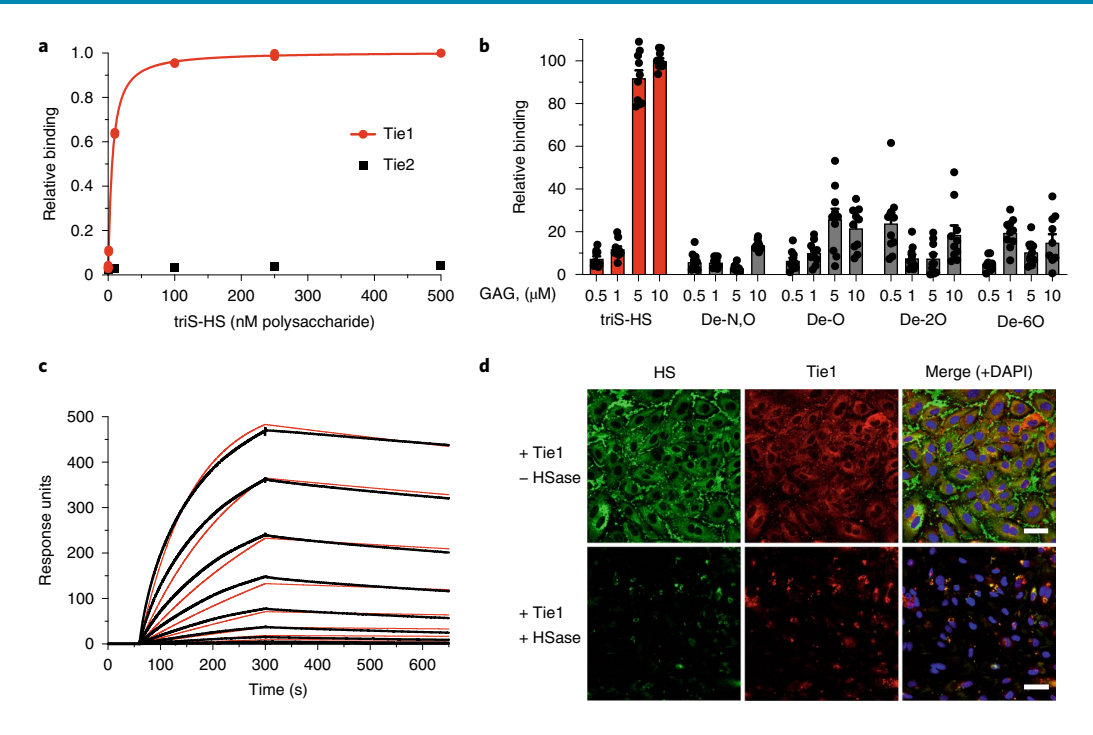


**Fig. 3** | The orphan receptor Tie1 binds to the trisulfated motif of HS. a-c, Binding was demonstrated by ELISA (a), glycan microarray (b) and SPR (c). Dissociation constant for Tie1, as determined by ELISA:  $K_{D,app} = 6.16 \, \text{nM}$  (5.40 to 7.01 nM); graphed data represent n = 2 independent replicates. This value is similar to dissociation constants reported for other GAG-protein interactions<sup>33,37</sup>. For glycan microarrays, data represent the mean  $\pm$  s.e.m.; n = 10 individual spots per glycan concentration. Dissociation constant for Tie1, as determined by SPR:  $K_{D,app} = 3.14 \, \text{nM}$  (3.12 to 3.15 nM). SPR data were fit using a 1:1 Langmuir model (red). d, Immunofluorescence images of HS GAGs (green) and Tie1-Fc ectodomain (red) binding to HUVECs treated with or without heparinase (HSase); scale bar:  $50 \, \mu \text{m}$ . Nuclear staining by DAPI (blue). Images are representative of three biologically independent samples.  $K_{D,app}$  values represent the mean (95% CI).

Sulfated GAGs are ligands for the orphan receptor Tie1. In addition to recruiting ligands to the cell surface, GAGs have been shown to directly engage transmembrane receptors 16,33,36,37. Consistent with the microarray results (Fig. 1c,d), no direct interaction was observed between triS-HS GAGs and Tie2 receptors using our modified ELISA (Fig. 3a). However, the orphan receptor Tie1 bound to tri-HS with nanomolar affinity ( $K_{D,app}$  of 6.16 nM, 95% confidence interval (CI): 5.40 to 7.01 nM; Fig. 3a). Interestingly, Tie1 also bound to the disulfated chondroitin sulfate-E (CS-E) motif (Extended Data Fig. 2a,b). To study the importance of the GAG sulfation pattern further, we assessed Tie1 binding to a panel of sulfated GAGs. The soluble Tie1-Fc ectodomain showed strong binding to both triS-HS and CS-E-enriched polysaccharides (Fig. 3b and Extended Data Figs. 2c and 3). Notably, loss of any sulfate group on HS or CS caused a significant decrease in binding, demonstrating the requirement of these sulfation motifs for Tie1 binding. Surface plasmon resonance (SPR) experiments using immobilized GAGs revealed apparent dissociation constants for Tiel-GAG interactions in the nanomolar range, comparable to those obtained by ELISA (Fig. 3c and Extended Data Fig. 2d).

To identify the physiologically relevant binding motif, we examined whether Tiel interacts with endogenous GAGs on HUVECs. As Tiel is most highly expressed during embryonic and early postnatal development<sup>29</sup>, the glycocalyx of HUVECs likely mimics the carbohydrate structures encountered by Tiel during development. We found that Tiel showed robust binding to HUVECs (Fig. 3d and Extended Data Fig. 4). Importantly, this binding was nearly abolished when HUVECs were pretreated with heparinase to remove endogenous HS GAGs, suggesting that HS GAGs are the major carbohydrate binding partner of Tiel on endothelial cells. Our results

are consistent with a previous report that HUVECs display more of the triS-HS motif than all CS motifs combined<sup>38</sup>, although it is possible that Tie1 may encounter and bind to CS-E in other physiological contexts.

Sulfated GAGs bind the N-terminal Ig-like domain of Tiel. To explore the molecular basis of the GAG-Tiel interaction, we expressed and purified a C-terminal truncation of the Tiel ectodomain lacking its three FN3 domains (Tiel-N; Extended Data Fig. 5a,b). We found that this Tiel-N construct maintained similar binding affinity for sulfated GAGs compared to the wild-type construct (Tiel-WT; Extended Data Fig. 5c,d), indicating that HS GAGs engage the N-terminal region of the protein.

To map the Tie1-GAG binding site, we turned to our GAG-Dock computational method, which has successfully predicted the interactions of sulfated GAGs with protein receptors<sup>39</sup>. Although no crystal structure of Tiel exists, Tiel shares 41.6% overall sequence identity with Tie2, along with the same predicted domain structure (Extended Data Fig. 6a). In accordance with previous studies27, we generated a structural homology model of the Tie1 N terminus based on a crystal structure of the Tie2 ectodomain<sup>40</sup> using SWISS-MODEL (Fig. 4a). The electrostatic potential surface of Tie1 revealed a large electropositive region centered on the first immunoglobulin-like (Ig-like) domain of Tie1 (Fig. 4b). In contrast, this strong electropositive region was absent from Tie2 (Extended Data Fig. 6b). We computationally sampled possible binding sites in the Tie1 structure using a triS-HS hexasaccharide and ranked the docked poses according to the calculated binding energies. The top ten binding poses of the hexasaccharide all localized to a single electropositive region within the first Ig-like domain

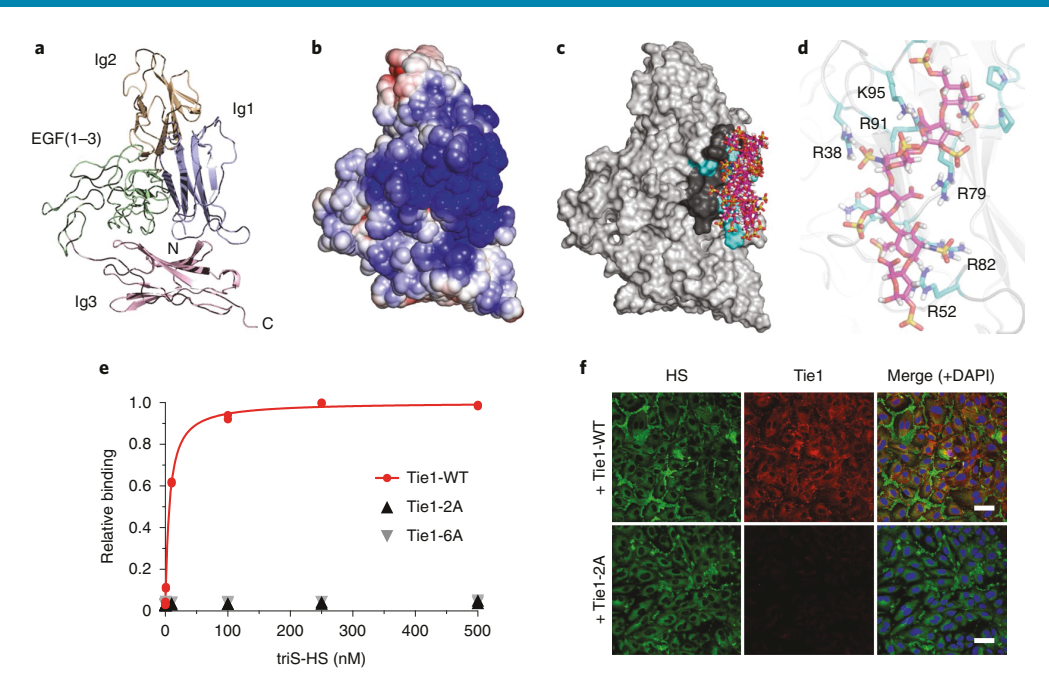


Fig. 4 | HS engages Tie1 within its first Ig-like domain (Ig1). a,b, Ribbon diagram (a) and electrostatic potential surface (b) of the N-terminal Tie1 homology model produced by SWISS-MODEL. The red to blue scale in b represents relative electrostatic potential (electronegative to electropositive). c, Superimposition of the top ten binding poses of triS-HS hexasaccharides (pink), ranked by calculated binding energies from GAG-Dock. d, Groove of six electropositive residues within 5-10 Å of the top ten docked triS-HS hexasaccharide poses. The top ranked pose is shown. e, Carbohydrate-ELISA binding assay for Tie1-WT and mutants (2A: R38A, R82A; 6A: R38A, R52A, R79A, R82A, R91A and K95A). Dissociation constant for Tie1-WT: K<sub>Dapp</sub> = 6.51nM (5.58 to 7.63 nM). Data represent the mean (95% CI); n=2 independent replicates. f, Immunofluorescence imaging of HUVECs with cell-associated HS GAGs (green) and soluble Tie1-WT or Tie1-2A (red); scale bar: 50 μm. Nuclear staining by DAPI (blue). Images are representative of three biologically independent samples.

(Fig. 4c). The energetic contributions from Coulombic forces dominated over hydrogen bonding and van der Waals forces in all ten poses (Extended Data Fig. 7a). Consistent with the importance of ionic interactions, Tie1 binding to heparin-Sepharose diminished with increasing salt concentration and was abolished by 0.8 M NaCl (Extended Data Fig. 7b).

Close inspection of the docked hexasaccharides revealed that all of the glycan structures were within 5–10 Å of six positively charged amino acid residues (R38, R52, R79, R82, R91 and K95; Fig. 4d and Extended Data Fig. 6c). Four of these residues are conserved across mammals, suggesting that this interaction may play a critical, evolutionarily important role (Supplementary Fig. 2). Moreover, only one of the six electropositive residues (K95) is conserved between Tie1 and Tie2, underscoring the specificity of HS for Tie1. Interestingly, the HS binding site is located ~30 Å away from one of the two reported Tie2 binding sites<sup>27,28</sup>, suggesting the potential for HS to modulate Tie1-Tie2 interactions (Extended Data Fig. 6d). Based on these findings, we generated two Tie1 constructs, in which all six residues (Tie1-6A) or only two central, conserved residues (R38 and R82; Tie1-2A) were mutated to alanine. Both mutant proteins were expressed and secreted from HEK-293T cells in equivalent amounts compared to Tie1-WT, consistent with proper folding and processing of the proteins (Extended Data Fig. 6e). As anticipated from our computational model, we found that both mutants lost all affinity for triS-HS (Fig. 4e). Moreover, Tie1-2A showed minimal binding to HUVECs (Fig. 4f), further indicating that our GAG-Dock method accurately predicted the residues necessary for the HS-Tie1 interaction.

**HS-Tie1 binding promotes Tie1 and Tie2 heterodimerization.** To elucidate the biological functions of the HS-Tie1 interaction, we examined whether this interaction altered the heterodimerization

of Tie1 and Tie2 (refs. 27,28). The Tie1-Tie2 heterodimer has been reported to be transient and difficult to detect, thus requiring the use of crosslinking agents<sup>26,27</sup>. We first treated HUVECs with the cell-impermeable, cleavable crosslinker 3,3'-dithiobis(sulfosucc inimidylpropionate) (DTSSP) to capture transient interactions between cell-surface receptors, then immunoprecipitated Tie1 and blotted for copurifying Tie2. Consistent with previous studies<sup>26,27</sup>, the relatively transient Tie1-Tie2 heterodimer was detectable only upon crosslinking. Notably, heparinase treatment of HUVECs before crosslinking led to a moderate but statistically significant decrease in coimmunoprecipitated Tie2 (Fig. 5a,b). To confirm these results using an independent method, we developed a proximity ligation assay41 to observe Tie1-Tie2 heterodimers directly at the cell surface. Here, we again observed a decrease in the amount of Tie1-Tie2 heterodimers after heparinase treatment (Fig. 5c,d). Together, these data suggest that the HS-Tie1 interaction helps to promote or stabilize Tie1-Tie2 heterodimers. Moreover, our proximity ligation assay provides a new approach to directly observe transient Tie1-Tie2 interactions.

HS-Tie1 promotes pathway activation and vascularization. Lastly, we assessed the functional importance of the HS-Tie1 interaction in vivo. As complete knockout of either Tie1 or HS GAGs results in embryonic lethality in mice and disrupts multiple aspects of their function<sup>12,22,23</sup>, we utilized CRISPR-Cas9 technology to selectively disrupt the HS-Tie1 interaction in mice. Briefly, homology-directed recombination with a double-stranded DNA donor template was used to mutate R38 and R82 in the endogenous Tie1 gene to alanine (Fig. 6a and Extended Data Fig. 8a). We also included silent mutations to remove the NGG protospacer adjacent motif and introduce restriction enzyme sites for facile genotyping (Extended Data

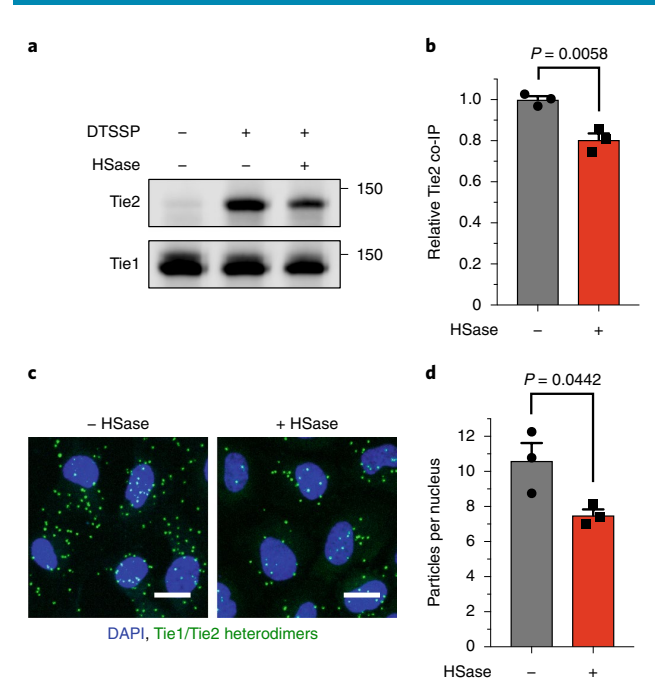


**Fig. 5 | Loss of the HS-Tie1 interaction decreases Tie1-Tie2 heterodimerization. a,b**, Representative western blots (**a**) and quantification (**b**) of Tie2 coimmunoprecipitation (co-IP) by Tie1 from HUVECs after treatment with or without heparinase (HSase) and chemical crosslinking. Coimmunoprecipitated Tie2 values were normalized to the corresponding Tie1 levels and are reported relative to the non-HSase-treated control. Data represent the mean $\pm$ s.e.m.; n=3 biologically independent samples; unpaired, two-tailed Student's t-test. **c,d**, Representative images (**c**) and quantification (**d**) of Tie1 and Tie2 heterodimers (green) revealed by proximity ligation assay from HUVECs with and without HSase treatment; scale bar:  $20 \, \mu$ m. Nuclear staining by DAPI (blue). Data represent the mean $\pm$ s.e.m.; n=3 biologically independent samples; unpaired, two-tailed Student's t-test.

Fig. 8b). The resulting Tie1-2A allele exhibited Mendelian inheritance ( $\chi^2$ =0.87, P>0.5). When heterozygous mice were crossed, mice homozygous for the Tie1-2A allele did not show embryonic lethality as observed for Tie1 knockout animals. No obvious difference in gross phenotype was observed between homozygous mutant mice and their wild-type littermates, although a slight decrease in overall weight was observed in adult homozygous mutant mice (Extended Data Fig. 8c).

To examine whether loss of the HS–Tie1 interaction in vivo led to alterations in the blood vasculature, we investigated postnatal retinal vascularization<sup>29</sup>. Retinas of pups from postnatal day 7 were fluorescently labeled with the endothelial-specific isolectin GS-IB<sub>4</sub>, and the distance that blood vessels grew from the optic disc was quantified. We found that retinas from the Tie1-2A animals displayed increases in radial outgrowth, vessel area and branching (Fig. 6b–d and Extended Data Fig. 8d,e), indicating that loss of HS–Tie1 binding had perturbed vascularization of the retina.

As Tie1 is highly expressed in the vascularized tissue of the lungs throughout development and into adulthood<sup>42</sup>, we also examined adult lung tissue for differences induced by loss of the HS-Tie1 interaction in vivo. We observed a robust decrease in Tie1 protein expression levels in adult Tie1-2A mice relative to the wild-type animals (38.5% ±7.9%; Fig. 6e,f), indicating that the HS-Tie1 interaction may be necessary for stable expression of Tie1 in vivo. Notably,

no differences in Tie1-WT and Tie1-2A protein levels were detected upon heterologous expression in cultured cells (Extended Data Fig. 6e and Supplementary Fig. 3), suggesting that the observed decrease in vivo was not caused by the misfolding or inherent instability of Tie1-2A. The Tie1-2A mice also exhibited a decrease in Tie2 protein expression levels (18.7%  $\pm$  6.2%; Fig. 6g) and a substantial decrease in Tie2 phosphorylation levels relative to the wild-type mice (51.6%  $\pm$  2.5%; Fig. 6h). Moreover, we detected a reduction of basal Akt phosphorylation levels in lung tissue from mutant mice compared to the wild-type mice (19.1% ± 4.3%; Fig. 6i), indicative of a decrease in downstream signaling through Tie2. Although decreases in Akt phosphorylation could result from changes in both endothelial and non-endothelial tissues, non-endothelial Akt is not expected to be affected by the Tie1-2A mutation as Tie1 and Tie2 are endothelial-specific proteins<sup>20,21</sup> and have not been reported to modulate Akt signaling outside of endothelial tissue. The reduction was specific to the Tie2-Akt signaling pathway, as levels of phospho-Erk1/2 remained unchanged between the genotypes (Extended Data Fig. 9). Together, these results provide strong evidence for an overall decrease in Ang-Tie pathway activation and prosurvival signaling in Tie1-2A mice.

#### Discussion

In this work, we demonstrate that HS GAGs are key regulators of the Ang–Tie signaling axis. Our studies indicate that HS GAGs bind to Ang1 and Ang4 with nanomolar affinity and form active ternary HS–Ang–Tie2 complexes (Extended Data Fig. 10a). Additionally, we discovered that HS GAGs directly interact with Tie1 receptors and stabilize Tie1–Tie2 heterodimer formation (Extended Data Fig. 10b). Through these dual mechanisms, HS GAGs potentiate Ang–Tie pathway signaling, revealing new modes of Ang–Tie pathway regulation.

The interaction of HS GAGs with Ang ligands highlights a common theme used by GAGs to direct cellular signaling. HS GAGs have been previously shown to recruit numerous soluble vascular growth factors to the cell surface, including VEGF<sub>165</sub> (refs. <sup>4,15</sup>), FGF2 (refs. <sup>5,16</sup>) and PDGF-BB<sup>18</sup>. The assembly of activated HS-ligand-receptor complexes has also been implicated in the rheostatic regulation of these RTK signaling pathways during sprouting angiogenesis <sup>16,18,36</sup>. Thus, our work extends a conserved process of ligand and receptor recruitment by GAGs to a new signaling pathway that is important for late stages of vascular development.

On the other hand, the discovery that HS GAGs bind to the Tie1 receptor highlights an alternative mechanism that has only recently emerged for the regulation of cellular signaling by GAGs. The ability of GAGs to engage cell-surface receptors directly and control downstream signaling, independent of the canonical ligands, is exemplified by the receptor protein tyrosine phosphatase PTP $\sigma$ , whose interaction with CS or HS GAGs inhibits or stimulates neuronal growth, respectively<sup>33,43</sup>. GAGs have also been demonstrated to bind to cell-surface receptors that indirectly modulate signaling, such as VEGFR1 (refs. 37,44) and neuropilin-1 (ref. 45). Our observation that the HS-Tie1 interaction affects Tie1-Tie2 heterodimerization and downstream signaling indicates that HS binding to cell-surface receptors can modulate signal transduction by altering the populations of receptor complexes. More broadly, these results reveal diverse mechanisms by which GAGs orchestrate signaling events at the cell surface beyond simple ligand recruitment.

Tie1–Tie2 heterodimer formation has been reported to occur at two distinct protein interfaces: (1) the multidomain N-terminal regions<sup>27</sup> and (2) the third FN3 domains of Tie1 and Tie2 (ref. <sup>28</sup>). We found that HS binds to an electropositive region in the first Ig-like domain of Tie1, adjacent to the N-terminal region interface. The proximity of the HS binding site to one of the two Tie1–Tie2 interfaces may account for the ability of HS to modulate Tie1–Tie2 interactions. The phenotypes observed in the Tie1-2A mice are

**ARTICIFS** 

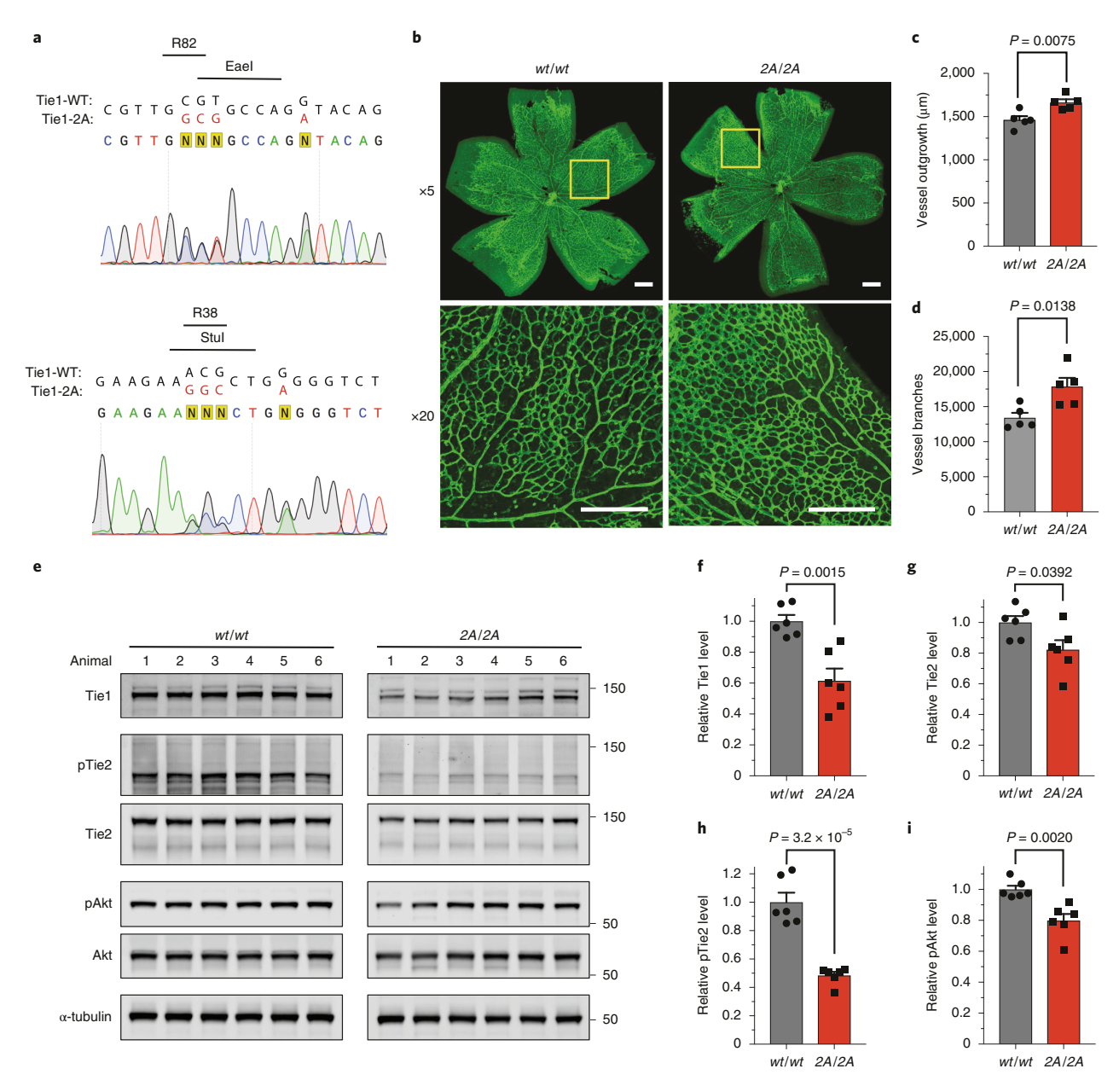


**Fig. 6 | Ablation of the HS-Tie1 interaction in vivo causes aberrant retinal vascularization and loss of endothelial prosurvival signaling. a**, Sequencing results from a heterozygous  $Tie1^{2A/wt}$  mouse. Mutated nucleobases (red) with the mutated amino acid residues, newly generated restriction enzyme sites and removed NGG protospacer adjacent motifs are displayed above the sequence. **b-d**, Representative images (**b**) and quantification (**c** and **d**) of retinal blood vessel radial outgrowth and vessel branching from 7-day-old Tie1-2A and wild-type littermates using GS-IB<sub>4</sub> (green); scale bar: 200 μm. n = 5 retina per genotype. **e-i**, Western blotting (**e**) and quantification (**f-i**) of total protein and phosphoprotein levels within the Ang-Tie pathway using lung tissue samples from  $Tie1^{2A/2A}$  and wild-type 4-month-old littermates; n = 6 animals per genotype. All protein levels are normalized to the corresponding α-tubulin loading control, and all phosphoprotein levels are normalized to the corresponding total protein level. All gels were transferred to the same blot and imaged to allow for direct comparisons between samples. Data are reported relative to the wild-type control. All data represent the mean ± s.e.m.; unpaired, two-tailed Student's t-test.

consistent with the notion that HS GAGs provide an additional level of control over the context-specific activity of Tie1. Interestingly, the Tie1-2A mice survived to adulthood in contrast to the embryonic lethality of Tie1 knockout mice<sup>22,23</sup>, and they exhibited milder defects in retinal angiogenesis than those reported for complete Tie1 and/or Tie2 knockouts<sup>29,31</sup>. Given that loss of the HS-Tie1

interaction only partially affected Tie1–Tie2 heterodimerization (Fig. 5), it is not unexpected that the Tie1-2A mutation produced milder phenotypes overall. Indeed, incomplete Tie1 knockout of up to 85% was previously reported to cause no significant retinal phenotypes<sup>31</sup>, consistent with the milder phenotypes of the Tie1-2A mice and suggesting that compensatory effects likely exist

to ameliorate vascular defects in vivo. We also observed an increase in vascularization, in contrast to the hypovascularization reported upon complete Tie1 knockout<sup>29,31</sup>. This finding reinforces previous studies showing that Tie1 both positively and negatively regulates Tie2 signaling in a context-specific manner and indicates that loss of HS–Tie1 binding disrupts the balance of Tie2 signaling differently from complete Tie1 knockout. Taken together, our studies suggest that HS functions as a rheostat to tune signaling through the Ang–Tie pathway and balance new vessel growth with vascular maturation and homeostasis.

Exciting questions remain regarding the assembly and overall structure of these newly discovered complexes. The exact structural organization of these and other GAG-ligand-receptor complexes remains elusive (Supplementary Fig. 4a). With the exception of the HS-FGF-FGFR complex<sup>16,17</sup>, structures of GAG-ligandreceptor complexes have not been solved. Nonetheless, our results suggest that the HS-Ang-Tie complex may resemble the HS-VEGF-VEGFR2 complex, wherein HS is predicted to interact primarily with the ligand (Supplementary Fig. 4b)37. Similarly to our biochemical observations, the VEGFR2 receptor was shown not to bind immobilized HS, but VEGFR2 could be recruited to HS in the presence of VEGF<sup>37</sup>. However, it is possible that weak interactions between HS and Tie2 receptors may exist but were not detected by our ELISA and microarray techniques, which utilized stringent wash conditions to minimize nonspecific binding. As such, the HS-Ang-Tie2 complex may also share similarities with the HS-FGF2-FGFR1 complex (Supplementary Fig. 4c)<sup>16,17</sup>. In this complex, HS binds within a groove that spans both the ligand and receptor and engages in contacts with both proteins (Supplementary Fig. 4d), although studies have shown that HS binds to FGF2 with much greater affinity than FGFR1 (ref. 46). In addition to studying the ternary complex structure, it will be interesting to determine whether HS chains participate in higher-order receptor clustering, which has been implicated in signal transduction through RTKs such as Tie2 (ref. <sup>28</sup>). Future studies using cryo-EM or super-resolution microscopy may help to illuminate the roles of HS in RTK signalosome assembly at the cell surface.

Despite accruing evidence that GAGs mediate many signal transduction events, their precise roles are only beginning to be understood due to the challenges of identifying and studying GAGprotein interactions. Here, we have developed an integrated chemical biology-based platform to discover new GAG-protein interactions and elucidate their complex functions. The rapid screening and characterization of GAG-protein interactions using GAG microarrays, ELISA-based assays and SPR, combined with computational modeling and mutagenesis to identify the binding interface, enable investigations into the function of the interaction. The development of glycan engineering techniques<sup>47</sup> allows for dissection of GAG function through the installation of defined carbohydrate structures at the cell surface, providing a much-needed, gain-of-function approach to complement traditional, loss-of-function techniques involving degradative enzymes or genetic knockout. With CRISPR-Cas9 technologies, the role of specific GAG-protein interactions can now be directly interrogated in vivo. To our knowledge, the Tie1-2A mouse model is the first example where an individual glycan-protein interaction has been selectively disrupted in vivo. Perturbing a specific GAG-protein interaction using the approach herein effectively revealed the precise contributions of the GAG to pathway regulation and diverged from the phenotypes of total protein knockouts. This general strategy will advance a fundamental understanding of the regulatory roles of GAGs and other carbohydrates in vivo, particularly in complex systems that cannot be recapitulated in vitro or using complete gene deletions.

In conclusion, we have demonstrated that sulfated GAGs regulate vascular function via the Ang-Tie RTK pathway through both direct ligand and receptor engagement. By recruitment of Angl

or Ang4 and Tie1 stabilization, our results illustrate new mechanisms underlying the multifaceted regulation of cellular signaling and vascular physiology by HS GAGs. Given the emerging roles of the Ang–Tie RTK pathway in numerous vascular abnormalities during cancer, sepsis and diabetes, our findings may provide new approaches to target this pathway and ameliorate disease-associated vascular defects.

#### Online content

Any methods, additional references, Nature Research reporting summaries, source data, extended data, supplementary information, acknowledgements, peer review information; details of author contributions and competing interests; and statements of data and code availability are available at https://doi.org/10.1038/s41589-020-00657-7.

Received: 15 August 2019; Accepted: 20 August 2020; Published online: 5 October 2020

#### References

- Potente, M., Gerhardt, H. & Carmeliet, P. Basic and therapeutic aspects of angiogenesis. Cell 146, 873–887 (2011).
- Carmeliet, P. & Jain, R. K. Molecular mechanisms and clinical applications of angiogenesis. *Nature* 473, 298–307 (2011).
- Adams, R. H. & Alitalo, K. Molecular regulation of angiogenesis and lymphangiogenesis. *Nat. Rev. Mol. Cell Biol.* 8, 464–478 (2007).
- Simons, M., Gordon, E. & Claesson-Welsh, L. Mechanisms and regulation of endothelial VEGF receptor signalling. *Nat. Rev. Mol. Cell Biol.* 17, 611–625 (2016).
- Beenken, A. & Mohammadi, M. The FGF family: biology, pathophysiology and therapy. Nat. Rev. Drug Discov. 8, 235–253 (2009).
- Andrae, J., Gallini, R. & Betsholtz, C. Role of platelet-derived growth factors in physiology and medicine. *Genes Dev.* 22, 1276–1312 (2008).
- Capila, I. & Linhardt, R. J. Heparin-protein interactions. Angew. Chem. Int. Ed. Engl. 41, 391–412 (2002).
- Xu, D. & Esko, J. D. Demystifying heparan sulfate-protein interactions. Annu. Rev. Biochem. 83, 129–157 (2014).
- Poulain, F. E. & Yost, H. J. Heparan sulfate proteoglycans: a sugar code for vertebrate development? *Development* 142, 3456–3467 (2015).
- Bishop, J. R., Schuksz, M. & Esko, J. D. Heparan sulphate proteoglycans fine-tune mammalian physiology. *Nature* 446, 1030–1037 (2007).
- Olczyk, P., Mencner, L. & Komosinska-Vassev, K. Diverse roles of heparan sulfate and heparin in wound repair. Biomed. Res. Int. 2015, 549417 (2015).
- 12. Forsberg, E. & Kjellen, L. Heparan sulfate: lessons from knockout mice. J. Clin. Invest. 108, 175–180 (2001).
- Fuster, M. M. & Wang, L. Endothelial heparan sulfate in angiogenesis. Prog. Mol. Biol. Transl. Sci. 93, 179–212 (2010).
- Jakobsson, L. et al. Heparan sulfate in trans potentiates VEGFR-mediated angiogenesis. Dev. Cell 10, 625–634 (2006).
- Xu, D., Fuster, M. M., Lawrence, R. & Esko, J. D. Heparan sulfate regulates VEGF<sub>165</sub>- and VEGF<sub>121</sub>-mediated vascular hyperpermeability. *J. Biol. Chem.* 286, 737-745 (2011).
- Schlessinger, J. et al. Crystal structure of a ternary FGF-FGFR-heparin complex reveals a dual role for heparin in FGFR binding and dimerization. Mol. Cell 6, 743–750 (2000).
- Pellegrini, L., Burke, D. F., von Delft, F., Mulloy, B. & Blundell, T. L. Crystal structure of fibroblast growth factor receptor ectodomain bound to ligand and heparin. *Nature* 407, 1029–1034 (2000).
- Abramsson, A. et al. Defective N-sulfation of heparan sulfate proteoglycans limits PDGF-BB binding and pericyte recruitment in vascular development. Genes Dev. 21, 316–331 (2007).
- van Wijk, X. M. R. & van Kuppevelt, T. H. Heparan sulfate in angiogenesis: a target for therapy. Angiogenesis 17, 443–462 (2014).
- Augustin, H. G., Koh, G. Y., Thurston, G. & Alitalo, K. Control of vascular morphogenesis and homeostasis through the angiopoietin–Tie system. *Nat. Rev. Mol. Cell Biol.* 10, 165–177 (2009).
- Saharinen, P., Eklund, L. & Alitalo, K. Therapeutic targeting of the angiopoietin–Tie pathway. Nat. Rev. Drug Discov. 16, 635–661 (2017).
- Sato, T. N. et al. Distinct roles of the receptor tyrosine kinases Tie-1 and Tie-2 in blood vessel formation. *Nature* 376, 70–74 (1995).
- Puri, M. C., Rossant, J., Alitalo, K., Bernstein, A. & Partanen, J. The receptor tyrosine kinase Tie is required for integrity and survival of vascular endothelial cells. EMBO J. 14, 5884–5891 (1995).
- Kim, M. et al. Opposing actions of angiopoietin-2 on Tie2 signaling and FOXO1 activation. J. Clin. Invest. 126, 3511–3525 (2016).

- Partanen, J. et al. A novel endothelial cell surface receptor tyrosine kinase with extracellular epidermal growth factor homology domains. Mol. Cell. Biol. 12, 1698–1707 (1992).
- Saharinen, P. et al. Multiple angiopoietin recombinant proteins activate the Tie1 receptor tyrosine kinase and promote its interaction with Tie2. *J. Cell Biol.* 169, 239–243 (2005).
- Seegar, T. C. M. et al. Tie1–Tie2 interactions mediate functional differences between angiopoietin ligands. Mol. Cell 37, 643–655 (2010).
- Leppänen, V.-M., Saharinen, P. & Alitalo, K. Structural basis of Tie2 activation and Tie2-Tie1 heterodimerization. *Proc. Natl Acad. Sci. USA* 114, 4376–4381 (2017).
- Savant, S. et al. The orphan receptor Tie1 controls angiogenesis and vascular remodeling by differentially regulating Tie2 in tip and stalk cells. *Cell Rep.* 12, 1761–1773 (2015).
- Korhonen, E. A. et al. Tie1 controls angiopoietin function in vascular remodeling and inflammation. J. Clin. Invest. 126, 3495–3510 (2016).
- D'Amico, G. et al. Tie1 deletion inhibits tumor growth and improves angiopoietin antagonist therapy. J. Clin. Invest. 124, 824–834 (2014).
- La Porta, S. et al. Endothelial Tie1-mediated angiogenesis and vascular abnormalization promote tumor progression and metastasis. J. Clin. Invest. 128, 834–845 (2018).
- Brown, J. M. et al. A sulfated carbohydrate epitope inhibits axon regeneration after injury. Proc. Natl Acad. Sci. USA. 109, 4768–4773 (2012).
- Rogers, C. J. et al. Elucidating glycosaminoglycan-protein-protein interactions using carbohydrate microarray and computational approaches. *Proc. Natl Acad. Sci. USA.* 108, 9747–9752 (2011).
- Pulsipher, A., Griffin, M. E., Stone, S. E. & Hsieh-Wilson, L. C. Long-lived engineering of glycans to direct stem cell fate. *Angew. Chem. Int. Ed. Engl.* 54, 1466–1470 (2015).
- Powell, A. K., Fernig, D. G. & Turnbull, J. E. Fibroblast growth factor receptors 1 and 2 interact differently with heparin/heparan sulfate: implications for dynamic assembly of a ternary signaling complex. J. Biol. Chem. 277, 28554–28563 (2002).

- Teran, M. & Nugent, M. A. Synergistic binding of vascular endothelial growth factor-A and its receptors to heparin selectively modulates complex affinity. J. Biol. Chem. 290, 16451–16462 (2015).
- Li, G. et al. Glycosaminoglycanomics of cultured cells using a rapid and sensitive LC-MS/MS approach. ACS Chem. Biol. 10, 1303–1310 (2015).
- Griffith, A. R. et al. Predicting glycosaminoglycan surface protein interactions and implications for studying axonal growth. *Proc. Natl Acad. Sci. USA.* 114, 13697–13702 (2017).
- Barton, W. A. et al. Crystal structures of the Tie2 receptor ectodomain and the angiopoietin-2-Tie2 complex. *Nat. Struct. Mol. Biol.* 13, 524-532 (2006).
- Fredriksson, S. et al. Protein detection using proximity-dependent DNA ligation assays. Nat. Biotechnol. 20, 473–477 (2002).
- Taichman, D. B. et al. A unique pattern of Tie1 expression in the developing murine lung. Exp. Lung Res. 29, 113–122 (2003).
- Coles, C. H. et al. Proteoglycan-specific molecular switch for RPTPσ clustering and neuronal extension. Science 332, 484–488 (2011).
- Meyer, R. D., Mohammadi, M. & Rahimi, N. A single amino acid substitution in the activation loop defines the decoy characteristic of VEGFR-1/FLT-1. J. Biol. Chem. 281, 867–875 (2006).
- Vander Kooi, C. W. et al. Structural basis for ligand and heparin binding to neuropilin B domains. *Proc. Natl Acad. Sci. USA* 104, 6152–6157 (2007).
- Ibrahimi, O. A., Zhang, F., Hrstka, S. C. L., Mohammadi, M. & Linhardt, R. J. Kinetic model for FGF, FGFR and proteoglycan signal transduction complex assembly. *Biochemistry* 43, 4724–4730 (2004).
- Griffin, M. E. & Hsieh-Wilson, L. C. Glycan engineering for cell and developmental biology. Cell Chem. Biol. 23, 108–121 (2016).

**Publisher's note** Springer Nature remains neutral with regard to jurisdictional claims in published maps and institutional affiliations.

© The Author(s), under exclusive licence to Springer Nature America, Inc. 2020

#### Methods

Materials. All chemicals were obtained from MilliporeSigma unless otherwise noted. All reagents used for molecular biology were obtained from New England Biolabs unless otherwise noted. All primers were obtained from Integrated DNA Technologies. Recombinant proteins were purchased from R&D Systems and resuspended according to the manufacturer's specifications. TriS-HS natural heparin/HS polysaccharides were purchased from Neoparin and Amsbio as clinical-grade preparations. The triS-HS polysaccharide is >70% enriched in the trisulfated 2-O-, 6-O- and N-sulfation motif. All desulfated HS polysaccharides were commercially produced by chemical desulfation of triS-HS and were obtained from Neoparin. N-desulfated, N-acetylated HS was obtained from MilliporeSigma. The average molecular weight of all heparin/HS molecules is approximately 15kDa (~20-25 disaccharide units). CS-E-enriched polysaccharides isolated from squid cartilage were purchased from Seikagaku. The polysaccharides contain ~60% of the disulfated 4-O- and 6-O-sulfation motif and have an average molecular weight of approximately 70 kDa (~110-120 disaccharide units). Primary antibodies were obtained from Cell Signaling Technology, R&D Systems or MilliporeSigma unless otherwise indicated. All cell culture reagents and secondary antibodies were obtained from Thermo Fisher Scientific unless otherwise noted. The HEK-293T (CRL-3216) and EA.hy926 (CRL-2922) cell lines, as well as primary pooled HUVECs (PCS-100-013), were obtained from the American Type Culture Collection and used as received. B6SJL-F1/J (100012) and C57BL/6J (000664) mice were obtained from The Jackson Laboratory.

Molecular biology. All miniprep, maxiprep and gel extraction steps were conducted using Zymo kits (Genesee Scientific). Cloning was performed using the NEBuilder HiFi Cloning Master Mix (New England Biolabs) unless otherwise noted. Human Tiel cDNA was obtained from pDONR223-TIE1 plasmid (23946, Addgene). The Tiel extracellular domain excluding the native secretion signal (A21 to Q759) was cloned into a pcDNA3.1 vector (Thermo Fisher Scientific) containing an N-terminal Ig  $\kappa$ -leader sequence and C-terminal human IgG, Fc and  $6\times His$  tags. Truncation (Tiel-N: A21 to S431) and site mutation (Tiel-2A and Tiel-6A) constructs were generated using the Q5 site-directed mutagenesis kit (New England Biolabs). The transmembrane HTP construct was produced as previously described  $^{15}$ . To obtain the lentiviral construct, the HTP sequence was first cloned into the pENTR4 vector (17424, Addgene) and then transferred into the pLenti-CMV-Blast vector (17451, Addgene) using the Gateway LR Clonase kit (Thermo Fisher Scientific). The vectors pCAG-EGxxFP (50716, Addgene) and pX459 (62988, Addgene) were used to test guide RNA (gRNA) sequences.

Cell culture. EA.hy926 and HEK-293T cells were cultured in complete DMEM (DMEM with 10% FBS and 1x penicillin–streptomycin (P/S)). HUVECs were cultured using endothelial cell basal medium (EBM-2, Lonza) with EGM-2 Bulletkit additives (Lonza) and were used for experiments between zero and five passages. For serum starvation, EA.hy926 cells were cultured in DMEM with 0.5% FBS and 1x P/S. Cells were generally grown on plastic, tissue-culture-treated plates (Sarstedt) without any coating. For experiments, HUVECs or EA.hy926 cells were plated onto plastic dishes, glass-bottom 96-well plates or  $\mu$ -Slide VI 0.5 glass-bottom channel slides (80607, ibidi) precoated with 5  $\mu$ g/cm² of bovine fibronectin (MilliporeSigma) and  $10\,\mu$ g/cm² of rat tail collagen type I (MilliporeSigma). Plates were coated by incubation with proteins dissolved in sterile PBS for 1 h at 37 °C, followed by two rinses with sterile PBS, and were used immediately.

Western blotting. Protein samples were diluted with one-fourth volume of 4× SDS-PAGE loading buffer (200 mM Tris at pH 6.8, 400 mM DTT, 8% SDS, 40% glycerol and 0.4% bromophenol blue) and heated to 95 °C for 10 min. Samples were then loaded onto NuPAGE 4-12% Bis-Tris protein gels (NP0355BOX, Thermo Fisher Scientific) and resolved using 180 V at room temperature (RT) for 1 h. The molecular weight of protein targets was estimated using Precision Plus Protein Dual Color Standards (Bio-Rad). Gels were transferred onto Immobilion-FL PVDF membrane (IPFL00010, EMD Millipore) using 250 mA at  $4\,^{\circ}\text{C}$  for 1–1.5 h. Membranes were then blocked for 1 h at RT with either 5% BSA in TBST (50 mM Tris at pH 7.4, 150 mM NaCl and 0.1% Tween) for phosphoprotein detection, 1:1 mixture of LI-COR blocking buffer (LI-COR Biosciences) and TBS for goat primary antibodies, or 5% nonfat milk in TBST, depending on the manufacturer's specifications. Primary antibodies used for western blotting, dilutions and commercial sources are as follows: Rb anti-His-tag (1:1,000; 12698S, Cell Signaling Technology), Gt anti-Tie2 (1:200; AF313, R&D Systems), Gt anti-Tie1 (1:200; AF619, R&D Systems), Rb anti-Tie1 (1:1,000; 23111S, Cell Signaling Technology), Rb anti-phospho-Tie2 (1:200; AF2720, R&D Systems), Rb anti-phosphorylated-Akt (1:1,000; 9275S, Cell Signaling Technology), Ms anti-Akt (1:1,000; 9275S, Cell Signaling Technology), Ms anti-a-tubulin (1:2,000; T9026, MilliporeSigma), Rb anti-phospho-p44/42 MAPK/Erk1/2 (1:1,000; 9101S, Cell Signaling Technology) and Ms anti-p44/42 MAPK/Erk1/2 (1:1,000; 4696S, Cell Signaling Technology). Primary antibodies were diluted in the same buffer as the blocking step and incubated at 4 °C overnight with gentle rocking. Blots were rinsed three times with TBST before incubation with secondary antibodies. For all western blots, highly cross-adsorbed Gt anti-Ms, Gt anti-Rb or Dk anti-Gt secondary antibodies

conjugated to Alexa Fluor 680 or Alexa Fluor 790 (Thermo Fisher Scientific) were used at 1:10,000 dilution (0.2  $\mu g$  ml $^{-1}$ ) in the same buffer as the blocking step with incubation at RT for 1 h with gentle rocking. Blots were then washed three times for 5 min with TBST before imaging with the L1-COR Odyssey CLx. Data acquisition and quantification was performed using ImageStudio Software (ver. 5.2.5; L1-COR). If necessary, blots were stripped using NewBlot PVDF Stripping Buffer (L1-COR) according to the manufacturer's protocol.

Protein expression and purification. For each protein construct, five 15-cm plates of 90% confluent HEK-293T cells in 20 ml of complete DMEM were transfected with 20-30 µg of Tie1-WT, Tie1-N, Tie1-6A or Tie1-2A plasmids using poly(ethyleneimine) (PEI; 23966-2, Polysciences). Briefly, DNA was diluted in 2 ml of prewarmed, serum-free DMEM, and PEI (1 mg ml<sup>-1</sup> in sterile double-distilled water (ddH<sub>2</sub>O)) was added dropwise with vigorous shaking at a 3:1 w/w PEI/DNA ratio, DNA-PEI complexes were allowed to form for 20 min at RT and then added dropwise to each plate. After 24 h, the medium in each plate was replaced with DMEM containing 2% FBS, 1× P/S and 0.5× cOmplete protease inhibitor cocktail without ETDA (PIC; 11697498001, MilliporeSigma). At 3 d after transfection, the medium was harvested and centrifuged to remove cell debris. A new 20-ml aliquot of DMEM, 2% FBS,  $1 \times$  P/S was added, which was harvested 2 d later, centrifuged and combined with the first aliquot. The solution pH was adjusted to 8.0 using 2 M Tris (pH unadjusted), and the collected medium was rotated end-over-end for 2h at 4°C with 500 µl of Ni-NTA resin (30230, Qiagen) that had been prerinsed twice with PBS. The resin was separated from the medium by centrifugation and loaded onto a disposable Poly-Prep chromatography column (Bio-Rad). The resin was washed with 10 ml of phosphate wash buffer (100 mM sodium phosphate at pH 7.4, 300 mM NaCl and 10 mM imidazole), and protein was eluted with two 1-ml aliquots of elution buffer (50 mM sodium phosphate at pH 7.4, 150 mM NaCl and 250 mM imidazole). Elution samples were combined and the buffer exchanged by centrifugation with PBS. Samples were stored at 4°C for up to 1 week or flash frozen and stored at -20 °C. Multiple attempts using this protocol to express N-terminal truncation constructs were unsuccessful, producing low to undetectable amounts of protein by western blot analysis.

Carbohydrate enzyme-linked immunosorbent assays. Biotinylation of CS-E, HS and chemically desulfated HS polysaccharides was conducted as previously described33. ELISAs were generally performed using commercially available Ang1-His<sub>6</sub>, Ang2-His<sub>6</sub>, Ang4-His<sub>6</sub>, Tie1-Fc and Tie2-Fc conjugates (R&D Systems). For ELISAs of truncated or mutant Tie1 constructs, all proteins used in the experiments were overexpressed and purified from mammalian cells as described above. Wells of copper-coated (Ang1-4) or protein A/G-coated (Tie1 and Tie2) eight-well strips (Thermo Fisher Scientific) were rinsed twice with 200 µl of PBST (PBS+0.02% Tween-20) and then incubated with 100 µl of 10 µg ml<sup>-1</sup> of the protein of interest in PBS containing 1% BSA (Thermo Fisher Scientific) for 1 h at RT with gentle rocking. Wells were rinsed three times with PBST and then blocked with  $200\,\mu l$  of 5% BSA in PBS for 1 h at RT. During this incubation step, a dilution series of biotinylated CS-E or HS was separately prepared in PBS. Wells were again rinsed three times with PBST, and 50 µl of each GAG-containing solution was added to the wells. For experiments to detect the GAG-Ang-Tie2 ternary complex, Ang1 or Ang4 (10 µg ml-1) was also added at this step. Wells were incubated with GAG-containing solutions for 3 h at RT with gentle rocking, then rinsed four times with PBST and incubated with 100 µl of HRP-conjugated streptavidin (1:15,000 dilution in PBST; Thermo Fisher Scientific) for 1 h at RT with gentle rocking. Wells were again rinsed four times with PBST and then incubated with 100 µl of development solution (R&D Systems) for 15 min at RT in the dark. Reactions were quenched by the addition of 100 µl of 2 N aqueous H2SO4, and the absorbance was read at 450 nm. Assays were performed in duplicate for each concentration, and data were collected using a FlexStation 3 (Molecular Devices) operated with SoftMax Pro acquisition and analysis software (ver. 5: Molecular Devices), Values were reported as the mean  $\pm$  s.e.m.  $K_{\text{D,app}}$  values were calculated with Prism 7 (GraphPad) using the nonlinear curve fitting of specific binding with the Hill slope function, and their 95% CIs were calculated as asymmetrical values by Prism 7. For experiments with overexpressed purified proteins, protein concentrations were first normalized using the bicinchoninic acid (BCA) assay (Thermo Fisher Scientific) and then used as described above.

**GAG microarrays.** GAG microarrays were generated and used as previously described  $^{\bowtie}$ . Briefly, slides were blocked with 10% FBS in PBS for 1 h at RT. Stock solutions of Tie1-Fc, Tie2-Fc, Ang1 and Ang4 (2  $\mu$ M) were prepared in PBS containing 1% BSA. Blocked slides were washed once with PBS and slowly rocked with 150  $\mu$ l of 1% BSA in PBS containing 1  $\mu$ M Tie1-Fc for 2 h at RT. For ternary complex formation, 150  $\mu$ l of 1% BSA in PBS containing 1  $\mu$ M Tie2-Fc with or without 1  $\mu$ M of ligand (that is, 1  $\mu$ M Tie2-Fc  $\pm$ 1  $\mu$ M Ang1; 1  $\mu$ M Tie2-Fc  $\pm$ 1  $\mu$ M Ang4) was used immediately without previous incubation. Slides were washed three times with PBS and incubated with 1:5,000 Alexa Fluor 647-conjugated Gt anti-human Fc antibody (109-605-098, Jackson ImmunoResearch Laboratories) in 1% BSA in PBS for 1 h at RT in the dark with gentle rocking. Slides were then washed three times with PBS and twice with ddH<sub>2</sub>O and blown dry under a stream of filtered air. Arrays were scanned using a G2565BA DNA Microarray Scanner

(Agilent), and fluorescence was measured and quantified using GenePix software (ver. 5.0, Molecular Devices) with normalization against local background. Data processing was conducted using Microsoft Excel for Mac (ver. 16.16.2). The data represent the average of ten spots per concentration of polysaccharide.

Surface plasmon resonance. All experiments were conducted using a Biacore T200 instrument (GE Healthcare). A CM5 sensor chip (GE Healthcare) was first functionalized with streptavidin using the manufacturer's amine coupling protocol. Briefly, all flow cells of a CM5 sensor chip were incubated at a flow rate of 10 µl min<sup>-1</sup> with a 1:1 molar ratio of N-hydroxysuccinimide and 1-ethyl-3-(3-dimethylaminopropyl)carbodiimide for 3 min, followed by 1 µM of streptavidin in 0.01 M NaOAc pH 5.0 until the response rate leveled off (saturating the flow cell surface). The remaining reactive groups were quenched with ethanolamine. Solutions of biotinylated CS-E or HS were then each flowed over one of the four flow cells (CS-E: flow cell 2; HS: flow cell 4) at a flow rate of 10 µl min-1 to provide a response value of roughly 25 RU. As a control, an antibody specific to CS-E33,48 was flowed over the CS-E-containing flow cell and corresponding control cell at a flow rate of  $20\,\mu l \; min^{-1}$  to ensure successful loading of biotinylated GAG. To test binding of Tie1-Fc to the biotinylated GAGs, a twofold dilution series of Tie1-Fc (starting at 100 nM) was produced and flowed over the flow cells for 300 s at a rate of 20 µl min-1. Dissociation of Tie1-Fc was then monitored for 350 s using the same flow rate. Between each run, the surface was regenerated using 2.5 M MgCl<sub>2</sub> at a flow rate of 30 µl min<sup>-1</sup>. Response values are reported after subtraction of the control (-GAG) cell. Data were collected by and the resulting curves were fit to the 1:1 Langmuir binding model equation using Biacore T200 evaluation software (ver. 1; GE Healthcare). Although the naturally derived polysaccharides may have multiple, heterogeneous binding sites, the simple 1:1 binding model was conservatively chosen to avoid overfitting the data with a multivalent regression model. The 95% confidence intervals were estimated as the mean  $\pm 1.96 \times$  s.e.m.

Heparin affinity chromatography. Heparin-Sepharose (Abcam) was loaded into a Poly-Prep column (Bio-Rad) with a bed volume of 0.5 ml and equilibrated with loading buffer (10 mM HEPES at pH 7.0 and 0.1 M NaCl). Protein (1  $\mu g$ ) was loaded onto the column, and the column was washed twice with 0.5 ml of loading buffer. Protein was then eluted in 0.5-ml fractions using a stepwise gradient of increasing NaCl concentration in 10 mM HEPES at pH 7.0. Fractions were desalted and concentrated by buffer exchange into PBS using 3-kDa MWCO Amicon filters. Samples were processed by western blotting for Tiel as described above.

**Isoelectric point calculation.** The isoelectric point (pI) of proteins was calculated by inputting the FASTA sequence of the protein of interest without the signal peptide into the protein isoelectric point calculator (http://isoelectric.org), which aggregates and averages 15 different pI predictive algorithms.

Tie1 cell-surface binding. HUVECs were plated onto precoated 96-well glass-bottom plates at 50,000 cells per well in EGM-2 and grown overnight at 37 °C. Cells were rinsed once with PBS and then incubated for 3 h at 37 °C in the presence or absence of 0.5 U ml-1 heparinase I/III (MilliporeSigma) in serum-starved DMEM (0.5% FBS). Cells were rinsed once with ice-cold PBS and then fixed with 4% paraformaldehyde in PBS for 20 min at RT. Cells were rinsed three times with PBS and then blocked with 2% BSA and 10% normal goat serum (16210064, Thermo Fisher Scientific) in PBS for 1 h at RT. Cells were incubated overnight at 4°C with 1:400 Ms anti-HS (clone F58-10E4; 370255-S, Amsbio) and 10 µg ml<sup>-1</sup> of recombinant Tie1-WT or Tie1-2A in 1% BSA in PBS. Cells were then washed for 5 min three times with PBS and incubated with 1:1,000 Alexa Fluor 488-conjugated Gt anti-Ms IgG (A-11001, Thermo Fisher Scientific), 1:1,000 Alexa Fluor 647-conjugated Gt anti-human Fc (109-605-098, Jackson ImmunoResearch Laboratories) and 1 µg ml<sup>-1</sup> of DAPI (D9542, MilliporeSigma) in 1% BSA in PBS for 1 h at RT in the dark. Cells were rinsed three times with PBS and then visualized using an LSM 700 confocal microscope (Carl Zeiss) with a Plan-Apochromat ×10/0.45 M27 objective using ZEN software (ver. 8.1; Carl Zeiss). For acquisition of xz- and yz-plane cell sections, samples were imaged using a Plan-Apochromat ×63/1.4 oil immersion objective, and z-stacks were acquired with a slice distance of 0.335 µm. Images were acquired in ZEN software and processed in FIJI/ImageJ and deconvoluted using Diffraction PSF 3D and Iterative Deconvolve 3D plugins.

Structural modeling. The Tie1 homology model was constructed using the program SWISS-MODEL (accessed May 2016 at https://swissmodel.expasy.org/)\*9 with human Tie2 ligand-binding domain (PDB 2GY5)\*0 as a template and the sequence of human Tie1 (UniProt P35590). The Tie1 homology model was briefly minimized in vacuum using the DREIDING force field (ver. May 2016)\*0 to reduce steric clashes built into the model. Preparation of the carbohydrate structure and docking experiments were conducted using the GAG-Dock method with MPsim (ver. May 2016) for molecular modeling and SCREAM (ver. May 2016) for side chain optimization as previously described\*9.

Cell-surface crosslinking. Detection of Tie1 and Tie2 heterodimers by chemical crosslinking and immunoprecipitation was adapted from a previous protocol<sup>26</sup>.

HUVECs were gently trypsinized for 5 min at 37 °C with TrypLE Express (12604-013, Thermo Fisher Scientific) and resuspended in PBS and pelleted at 1,000g twice. Cells were then resuspended in serum-starved DMEM in the presence or absence of 1 U ml-1 of heparinase I/III for 2 h at 37 °C with gentle mixing every 15 min. Cells were plated on precoated six-well plates and grown overnight at 37 °C in EGM-2. On the following day, cells were rinsed three times with ice-cold PBS and then incubated with 100 µl of 1 mM DTSSP in PBS (freshly prepared) for 30 min at RT with gentle rocking. Unreacted DTSSP was quenched by addition of 5 µl of 1 M Tris (pH 8.0) with incubation for 15 min at RT. The crosslinking solution was then removed, and cells were lysed by scraping with 200 µl of ice-cold Triton lysis buffer (20 mM HEPES at pH 7.9, 150 mM NaCl, 1% Triton X-100, 5% glycerol and 1× PIC). Lysates were rotated end-over-end for 10 min at 4°C and then centrifuged for 10 min at 21,000g to remove all insoluble material. The lysates were transferred to new tubes, diluted to 500 µl with Triton lysis buffer and rotated end-over-end with 1:100 Gt anti-Tie1 (AF619, R&D Systems) overnight at 4°C. The next day, 20 µl of magnetic protein A/G beads (Thermo Fisher Scientific) prerinsed with HBS (50 mM HEPES pH 7.9 and 150 mM NaCl) was added to each sample, and the samples were rotated end-over-end for 1 h at 4 °C. Beads were then washed with 500 µl of HBS and 0.1% Triton X-100 three times for 5 min at 4 °C. After the final wash, all wash buffer was removed, and the beads were resuspended in  $30\,\mu l$  of  $1\times$  SDS-PAGE loading buffer and  $20\,mM$  DTT (freshly prepared) and heated to 95 °C for 10 min. Samples were processed by western blotting for Tie1 and Tie2 as described above. The assay was performed in triplicate. As a negative control for nonspecific binding, the coimmunoprecipitation protocol was also carried out without DTSSP treatment for each replicate. Coimmunoprecipitated Tie2 values were normalized to the total immunoprecipitated Tie1 levels and are reported relative to the non-heparinase-treated control. Statistical analysis was performed by Prism 7 using a paired, two-tailed Student's t-test.

Proximity ligation assays. HUVECs were treated in suspension in the presence or absence of heparinase I/III as described above. Cells were then plated at 50,000 cells per well onto precoated 96-well glass-bottom plates and grown overnight at 37 °C with EGM-2. On the following day, cells were washed twice with PBS and fixed with 4% paraformaldehyde in PBS for 20 min at RT. Cells were rinsed three times with PBS and blocked with the DuoLink blocking buffer (MilliporeSigma) for 1 h at RT. After rinsing twice with PBS, cells were incubated overnight at 4 °C with 1:100 Ms anti-Tie1 (MAB619, R&D Systems) and 1:100 Rb anti-Tie2 (H176, Santa Cruz Biotechnology) in 1% BSA in PBS. Cells were then carried through the Duolink labeling protocol scaled to 30 µl reactions per well according to the manufacturer's protocol (DUO92101, MilliporeSigma). Cells were mounted using DuoLink in situ mounting medium with DAPI (MilliporeSigma) and were visualized using an LSM 700 confocal microscope with a Plan-Apochromat ×40/1.4 oil immersion DIC M27 objective and preset filter settings for Texas Red and DAPI using ZEN software. A z-stack of images was collected for each field of view and combined to form a single maximum-intensity projection. Puncta depicted in Fig. 5 are pseudo-colored green for clarity. Nuclei and individual interaction puncta were quantified using FIJI/ImageJ (ver. 2.0.0-rc-43/1.51w; National Institutes of Health (NIH)). The assay was performed in triplicate. Data are reported as absolute values of the average number of puncta per nucleus. Statistical analysis was performed by Prism 7 using an unpaired, two-tailed Student's *t*-test.

**Lentivirus production.** Lentiviruses were produced by co-transfecting two to four 10-cm plates of 90% confluent HEK-293T cells in complete DMEM with the HTP lentiviral plasmid and pLP1, pLP2 and VSV-G packaging plasmids (Thermo Fisher Scientific) at 4.3, 6.2, 3.1 and 3.7  $\mu$ g, respectively, using Lipofectamine 3000 (Thermo Fisher Scientific) according to the manufacturer's protocol. Medium was harvested and replaced with complete DMEM at 24, 48 and 72 h, centrifuged to remove cell debris and combined. Lentivirus particles were either directly flash frozen and stored at  $-80^{\circ}$ C or concentrated by PEG-6000 precipitation as previously described  $^{51}$ . Precipitated lentiviruses were resuspended in complete DMEM, flash frozen and stored at  $-80^{\circ}$ C.

Generation and validation of EA.hy926-HTP cell line. EA.hy926 cells were grown to 80% confluency in a six-well plate with 2 ml of complete DMEM and then treated with 0-20 µl of the concentrated HTP lentivirus stock along with 8 µg  $ml^{-1}$  of polybrene (MilliporeSigma). After 48 h, cells were split 1:3 into new six-well plates in 2 ml of complete DMEM containing  $5\,\mu g\ ml^{-1}$  of blasticidin (InvivoGen). Medium was changed every 2 d until all cells in the untreated well had died (roughly 1-1.5 weeks). Cells were treated for an additional 3 d with 5 μg ml<sup>-1</sup> of blasticidin, and cells from the well treated with the lowest amount of lentivirus that survived selection were expanded and cryopreserved. To validate expression of HTP, treated and untreated £A.hy926 cells were plated onto precoated 96-well glass-bottom plates and grown to confluency. Cells were then treated with 1:1,000 cell-impermeable Alexa Fluor 488-conjugated CL (AF488-CL, G1001, Promega) and 1:1,000 Hoescht 33342 (H3750, Thermo Fisher Scientific) in complete DMEM at 37 °C for 15 min. Cells were rinsed three times with FluoroBrite DMEM (A18967, Thermo Fisher Scientific), and live-cell imaging was performed using an LSM 700 confocal microscope with a Plan-Apochromat ×10/0.45 M27 objective.

FOXO1 localization assay. The stimulation, detection and quantification of FOXO1 nuclear export were adapted from a previous protocol30. HUVECs were treated in suspension in the presence or absence of heparinase I/III as described above. Cells were then plated on precoated μ-Slide VI 0.5 glass-bottom channel slides (80607, ibidi) at 50,000 cells per channel and grown overnight at 37 °C with EGM-2. On the following day, the medium was replaced with serum-starved DMEM for 6 h. Before treatment, Ang1 was diluted to 400 ng ml-1 in serum-starved DMEM in the presence or absence of 20 µg ml<sup>-1</sup> of triS-HS and incubated for 30 min at 37 °C. The Ang1-containing medium was then added to the serum-starved HUVECs. After 15 min at 37 °C, cells were rinsed with ice-cold PBS and fixed with 4% paraformaldehyde in PBS for 20 min at RT. Cells were permeabilized with 0.1% Triton X-100 in PBS for 15 min at RT and blocked with PBS containing 2% BSA and 10% normal goat serum for 1 h at RT. Antibody staining was performed overnight by incubating with 1:100 Rb anti-FOXO1 (2880S, Cell Signaling Technology) in 1% BSA in PBS. Cells was washed for 5 min three times with PBS and then stained with 1:1,000 Alexa Fluor 568-conjugated Gt anti-Rb IgG (A11036, Thermo Fisher Scientific) and  $1\,\mu g\ ml^{-1}$  of DAPI in 1%BSA/PBS for 1h at RT in the dark. Cells were rinsed three times with PBS and then visualized using an LSM 700 confocal microscope with Plan-Apochromat ×10/0.45 M27 and ×20/0.45 M27 objectives. The number of DAPI-stained nuclei (>100 per condition per replicate) was quantified using FIJI/ImageJ (NIH), and FOXO1+ and FOXO1 nuclei were counted manually. The assay was performed in triplicate. Data are reported as the percentage of FOXO1<sup>-</sup> nuclei. Statistical analyses were performed in Prism 7 using a one-way ANOVA with Tukey's post hoc test.

Glycan engineering and stimulation assay. Cell surfaces were engineered with defined HS GAG structures using minor modifications to the published protocol35. A chlorohexyl linker was attached to the low-abundance glucosamine sugar of tri-HS and de-HS polysaccharides via reductive amination chemistry as reported35 to give triS-HS-CL and deS-HS-CL. EA.hy926-HTP cells were treated in suspension with heparinase I/III as described above. Cells were then plated on precoated six-well plates and grown overnight at 37°C with complete DMEM. On the following day, the medium was replaced with serum-starved DMEM containing  $5\,\mu g\,ml^{-1}$  of deS-HS-CL or triS-HS-CL. After 2 h, the medium was removed, and cells were treated with serum-starved DMEM for an additional 4 h. Cells were then stimulated with serum-starved DMEM containing  $500\,\mathrm{ng}\;\mathrm{ml}^{-1}$ of Ang1, Ang2, or Ang4 or no ligand for 30 min at 37 °C. Cells were rinsed with ice-cold PBS and then lysed with 200 µl of SDS lysis buffer (50 mM Tris at pH 7.6, 150 mM NaCl, 1% SDS, 1× PIC and 1× Phos-STOP (MilliporeSigma)) at RT. Lysates were sonicated for 10 s at 40% intensity to sheer DNA and then centrifuged for 5 min at 21,000g to remove any insoluble debris. Lysates were subjected to western blotting as described above. The assay was performed in triplicate. Phosphorylated-Akt values were normalized to total Akt levels and are reported as the average value normalized to the untreated deS-HS-CL control. Statistical analyses were performed in Prism 7 using a two-way ANOVA with Sidak's multiple-comparisons test.

General animal care and maintenance. All animal experiments were conducted according to protocols approved by the Caltech Institutional Animal Care and Use Committee. Animals were maintained with no more than five adult animals per cage in small mouse cages with enrichment under 20–26 °C ambient temperature, 30–70% relative humidity and a 12-h light–dark cycle. General animal maintenance and timed matings were performed by members of the Caltech Office of Laboratory Animal Resources with cage changes performed weekly.

Transgenic Tie1-2A mouse model generation. Guide RNA sequences were designed using the online CHOPCHOP tool (ver. 2; https://chopchop.cbu. uib.no/)52 against the Dec. 2011 (GRCm38/mm10) murine genome assembly against regions surrounding the Tie1 R38 and R82 codons. Sequences were selected based on predicted activity and minimal off-target homology. Candidate gRNA sequences were assayed as previously described<sup>53</sup>. Two gRNAs were selected to target R38 (CGCAGGTCAGGAAGAAACGC) and R82 (GGTGAGAACCGTTGCGTGCC) and purchased as Alt-R CRISPR RNA (crRNA) products (Integrated DNA Technologies) along with a double-stranded DNA (dsDNA) repair template GeneBlock (Integrated DNA Technologies) containing the R38A and R82A mutations, as well as silent mutations to insert StuI and EaeI restriction sites and remove the NGG PAM sequence. Reagents were prepared according to the manufacturer's suggested protocol. RNA molecules were dissolved in sterile injection buffer (1 mM Tris at pH 7.5 and 0.1 mM EDTA) at 1 µg  $\mu l^{-1}.$  Duplexes of each targeting crRNA and a trans-activating crRNA (tracrRNA) were produced by first combining 5 μl of 1 μg μl<sup>-1</sup> crRNA and 10 μl of 1 μg μl<sup>-1</sup> tracrRNA. Mixtures were incubated in a thermocycler at 95°C for 5 min and then ramped down to 25 °C at 5 °C per minute. Resulting duplexes were diluted twofold in injection buffer, and  $4\mu l$  of each duplex was combined with  $64\mu l$  of injection buffer. Cas9 protein (Integrated DNA Technologies) was diluted to 500 ng μl<sup>-1</sup> in injection buffer, and  $8\,\mu l$  of this Cas9 solution was added to the RNA mixture. Samples were incubated for 15 min at RT. The Cas9/gRNA mixture was aliquoted at  $20\,\mu l$ , and  $5\,\mu l$  of  $100\,ng\,\mu l^{-1}$  dsDNA repair template was added. Samples were centrifuged for 10 min at 21,000g, and 20 µl was transferred to a new tube. The

final concentrations of the injection solution were  $20\,\text{ng}\;\mu\text{l}^{-1}$  each of gRNA/Cas9 complex and 20 ng  $\mu l^{\scriptscriptstyle -1}$  of repair template. Pronuclear injections and subsequent culture and implantation steps were adapted from a previous protocol<sup>54</sup>. Roughly 300 zygotes from superovulated, mated B6SJL-F1/J mice were injected with the solution into one of the pronuclei. Zygotes that had proceeded to the blastocyst stage were implanted into surrogate B6SJL-F1/J mice, and viable offspring were tailed for genotyping. Three animals were obtained with one allele correctly modified, one of which was used to establish the colony. Animals were backcrossed for at least three generations with C57BL/6J mice before use. Genotyping was performed by first purifying genomic DNA from tail snips using the DNeasy Blood and Tissue kit (69504, Qiagen). PCR reactions (35 cycles at 66 °C annealing temperature and a 2-min extension time) were set up by combining the following: 12.5 µl of 2× Q5 Hot Start High Fidelity 2× master mix (M0494S, New England Biolabs), 8 μl of H<sub>2</sub>O, 2 μl of genomic DNA, 1.25 μl of 10 μM forward primer (5'-AGAGCTACAGATGAGAGGGAAG-3'), 1.25 μl of 10 μM reverse primer (5'-CACATTCTTCTCCTCGGTCTTG-3'). To each reaction, 1 µl of StuI (R0187S, New England Biolabs) was added, and the mixture was incubated at 37 °C for 1.5 h. Samples were diluted with 6× purple loading dye (B7025S, New England Biolabs) and resolved on a 1% agarose gel by application of a constant voltage of 120 V for 30 min. Bands were visualized using an Enduro GDS Touch gel imager (Aplegen).

Tissue harvesting and processing. Male and female mice were both used in all experiments except for direct weight comparisons. Tissue samples were acquired from littermates from at least two independent litters that were processed and analyzed together after genotyping. Retinal tissue harvesting, dissection and immunostaining with the Alexa Fluor 488-conjugated endothelial-specific isolectin GS-IB4 (I21411, Thermo Fisher Scientific) were performed as previously described29. Entire retinal areas and representative regions were imaged using an LSM 700 confocal microscope with a Plan-Apochromat ×5/0.16 M27 or Plan-Apochromat ×20/0.8 M27 objective, respectively; images were acquired using 4×4 or 5×5 tiling scans, respectively, with automatic stitching by ZEN software (Zeiss). All image analysis was performed using FIJI/ImageJ as previously described29. Vessel outgrowth was measured as the distance from the optic disc to the retinal front. Relative vessel area was calculated as the IB, area per entire retinal area. The number of branches and branchpoints were measured by skeletonizing the IB4-stained vessels of the entire retinal area and automated skeleton analysis via the AnalyzeSkeleton plugin of FIJI/ImageJ. Statistical analysis was performed by Prism 7 using an unpaired, two-tailed Student's t-test. Lung tissues were harvested from adult 4-month-old mice, rinsed with PBS and immediately lysed by douncing with 1 ml of ice-cold T-PER extraction reagent (78510, Thermo Fisher Scientific) containing 1× PIC and 1× Phos-STOP. Lysates were clarified by centrifugation at 16,000g for 10 min at 4 °C, and protein concentrations were quantified by BCA assay. Lysates were analyzed by western blotting as described above. Total protein levels were normalized to the corresponding a-tubulin protein loading control, and phosphoprotein values were normalized to the corresponding total protein level. All data are reported relative to the wild-type animal control. Statistical analyses were performed by Prism 7 using an unpaired, two-tailed Student's t-test.

**Reporting Summary.** Further information on research design is available in the Nature Research Reporting Summary linked to this article.

#### Data availability

Data generated or analyzed during this study are included in the article and related Supplementary Information or are available from the corresponding author on reasonable request. Publicly available data used in this study include the Tie2 crystal structure (PDB 2GY5), the Tie1 protein sequence (UniProt P35590), the Dec. 2011 murine genome assembly (GRCm38/mm10) and the CHOPCHOP gRNA design tool (https://chopchop.cbu.uib.no/). Source data are provided with this paper.

#### References

- Tully, S. E., Rawat, M. & Hsieh-Wilson, L. C. Discovery of a TNF-α antagonist using chondroitin sulfate microarrays. J. Am. Chem. Soc. 128, 7740–7741 (2006).
- Waterhouse, A. et al. SWISS-MODEL: homology modelling of protein structures and complexes. *Nucleic Acids Res.* 46, W296–W303 (2018).
- Mayo, S. L., Olafson, B. D. & Goddard, W. A. III DREIDING: a generic force field for molecular simulations. J. Phys. Chem. 94, 8897–8909 (1990).
- Kutner, R. H., Zhang, X.-Y. & Reiser, J. Production, concentration and titration of pseudotyped HIV-1-based lentiviral vectors. *Nat. Protoc.* 4, 495–505 (2009).
- Montague, T. G., Cruz, J. M., Gagnon, J. A., Church, G. M. & Valen, E. CHOPCHOP: a CRISPR-Cas9 and TALEN web tool for genome editing. *Nucleic Acids Res.* 42, W401–W407 (2014).
- Mashiko, D. et al. Generation of mutant mice by pronuclear injection of circular plasmid expressing Cas9 and single guided RNA. Sci. Rep. 3, 3355 (2013).

 Wang, H. et al. One-step generation of mice carrying mutations in multiple genes by CRISPR-Cas-mediated genome engineering. *Cell* 153, 910–918 (2013).

#### Acknowledgements

We thank S. Pease and staff of the Caltech Genetically Engineered Mouse Services Core for help with generating the Tie1-2A mouse line and J. Costanza and A. Gomez of the Caltech Office of Laboratory Animal Resources for mouse line care and maintenance. We also thank J. Vielmetter and the Caltech Protein Expression Center of the Beckman Institute for help with conducting the SPR experiments. This work was supported by the NIH (5R01GM093627 and 5R01GM127920 to L.C.H.-W.) and the National Science Foundation (CBET-1805022 to W.A.G., DGE-1144469 to M.E.G. and DGE-1745301 to A.W.S.).

#### **Author contributions**

M.E.G. and L.C.H.-W. conceived the project. Unless otherwise noted, M.E.G. performed the experimental work. A.W.S. conducted some of the microarray, ELISA and cell

imaging assays. G.M.M. aided in assay optimization for initial binding experiments and conducted all computational work under the guidance of W.A.G.III. All authors contributed to the design of the experimental and computational work and to data analysis, discussed the results and commented on the manuscript. M.E.G. and L.C.H.-W. wrote the manuscript. L.C.H.-W. supervised the project.

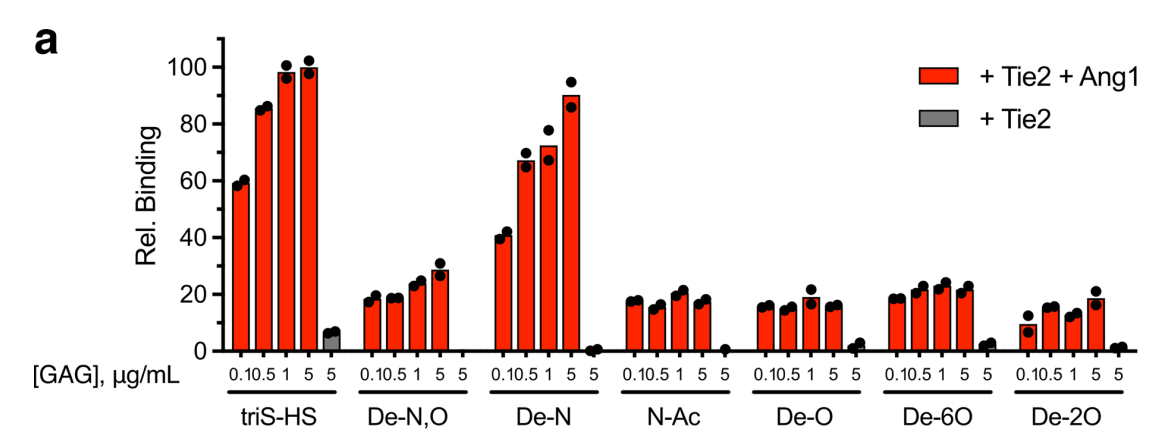
#### **Competing interests**

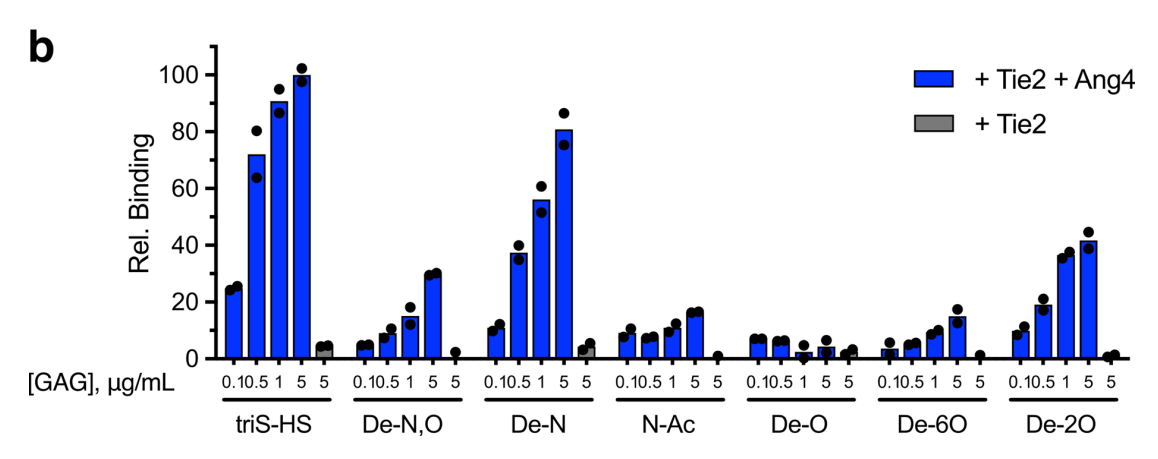
The authors declare no competing interests.

#### Additional information

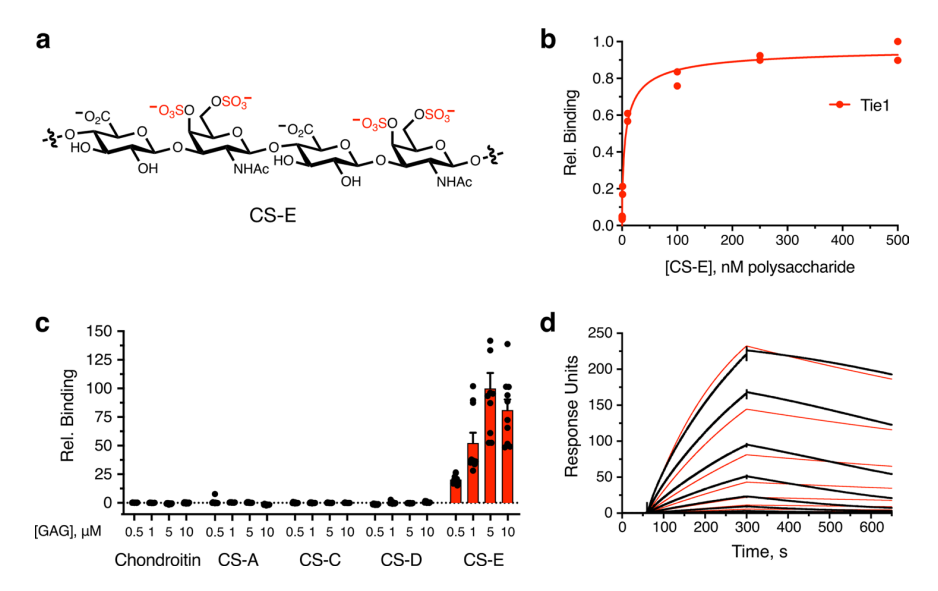
**Extended data** is available for this paper at https://doi.org/10.1038/s41589-020-00657-7. **Supplementary information** is available for this paper at https://doi.org/10.1038/s41589-020-00657-7.

Correspondence and requests for materials should be addressed to L.C.H.-W. Reprints and permissions information is available at www.nature.com/reprints.

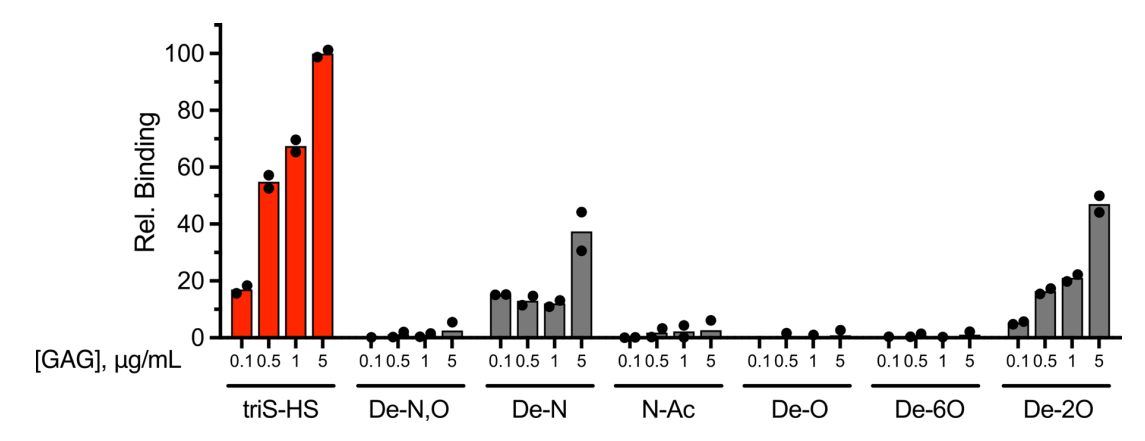




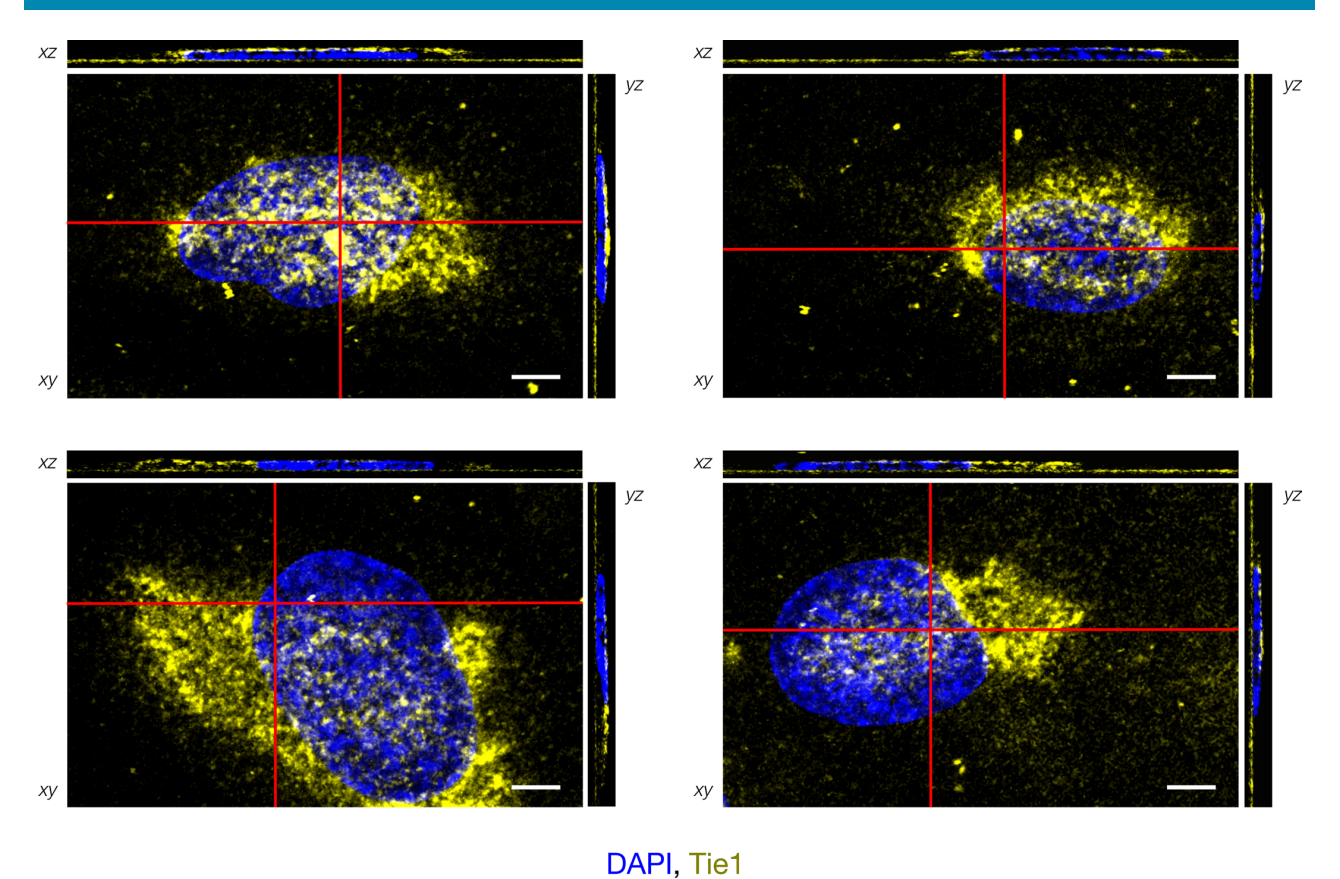
**Extended Data Fig. 1** | Ang-Tie2 complex formation occurs in a sulfation-dependent manner. Binding of biotinylated HS sulfation motifs to immobilized Tie2 in the presence or absence of **a** Ang1 or **b** Ang4, as detected by ELISA. Removal of the *N*- and *O*-sulfate groups (De-N,O), the *N*-sulfate groups (De-O), the 6-O-sulfate groups (De-O), or the 2-O-sulfate groups (De-2O), or conversion of the *N*-sulfate to *N*-acetyl groups (N-Ac) reduced formation of HS-Ang1/4-Tie2 ternary complexes. Data represent mean ± s.e.m.; n=2 independent replicates.



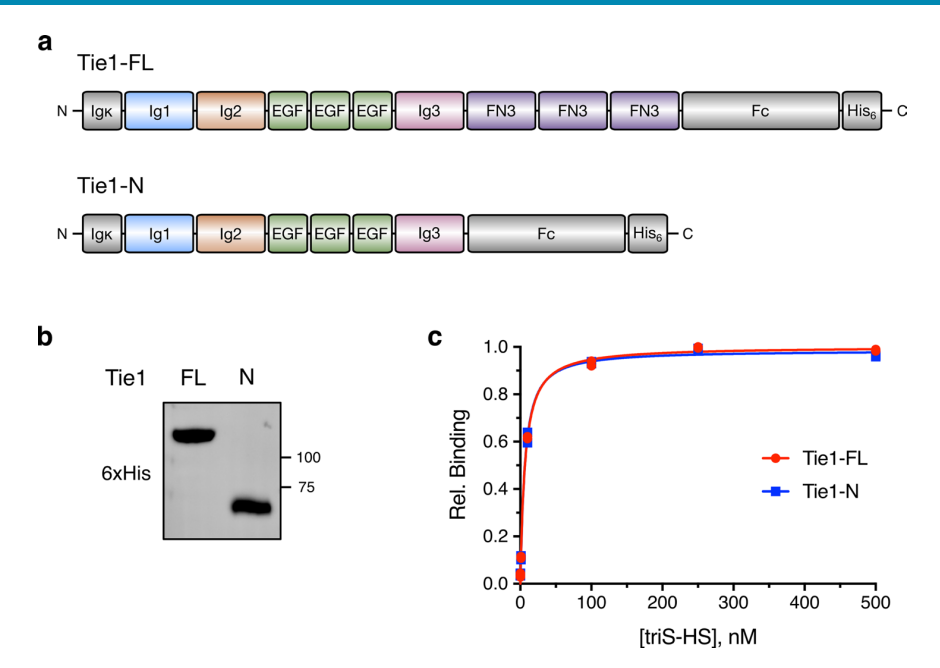
**Extended Data Fig. 2 | Orphan receptor Tie1 binds to the CS-E motif. a**, Chemical structure of the CS-E sulfation motif in CS polysaccharides. Interaction of CS-E and Tie1 by **b** ELISA, **c** glycan microarray, and **d** surface plasmon resonance. Dissociation constant for Tie1, as determined by ELISA:  $K_{Dapp} = 19.9 \text{ nM}$  (10.5 to 53.5 nM); value represents mean (95% CI); graphed data represent n = 2 independent replicates. For glycan microarrays, data represent mean  $\pm$  s.e.m.; n = 10 individual spots per glycan concentration. Dissociation constant for Tie1, as determined by SPR:  $K_{Dapp} = 14.7 \text{ nM}$  (14.6 to 14.8 nM); value represents mean (95% CI). SPR data were fit using a 1:1 Langmuir model shown in red.



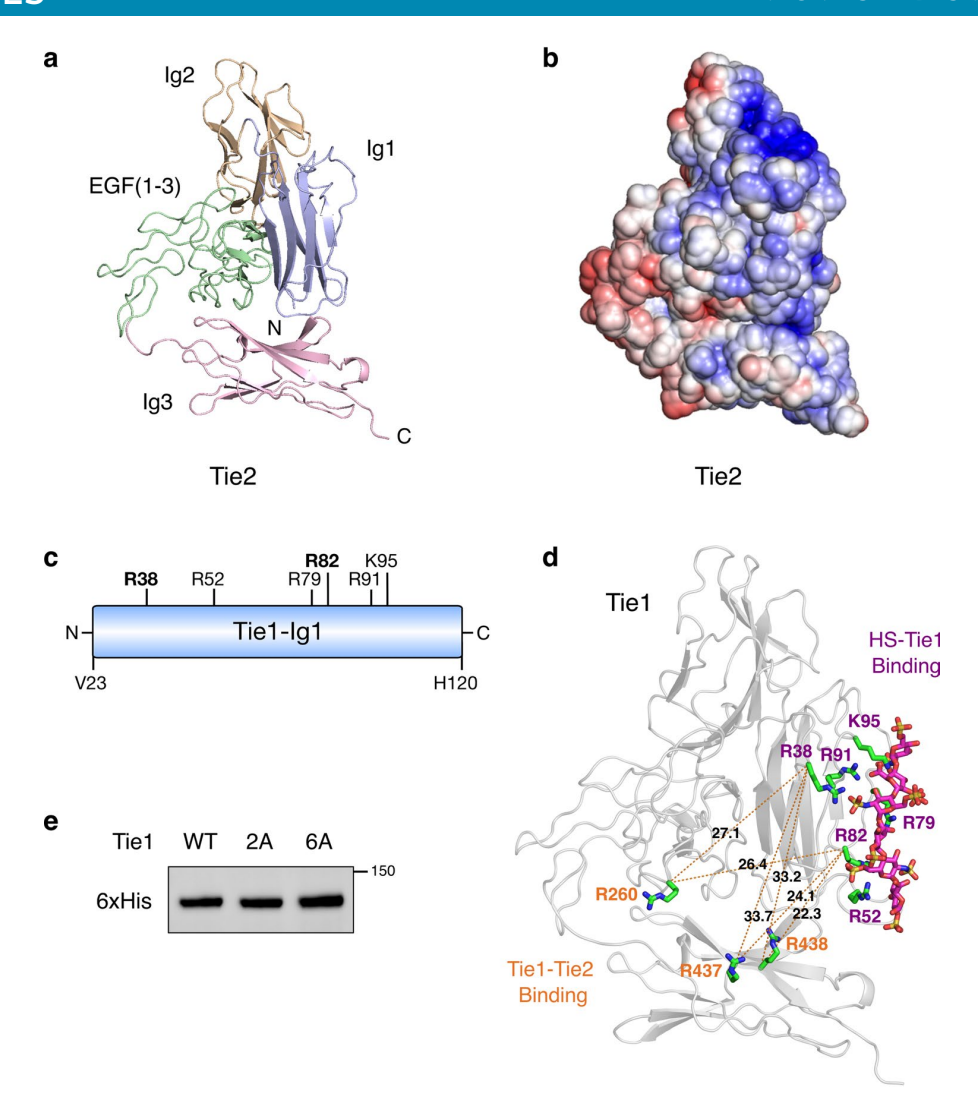
**Extended Data Fig. 3 | HS engages Tie1 in a sulfation-specific manner.** Binding of Tie1-Fc to different HS sulfation motifs, as determined by ELISA. Removal of the *N*- and *O*-sulfate groups (De-N,O), the *O*-sulfate groups (De-O), or the 6-O-sulfate groups (De-6O), or conversion of the *N*-sulfate to *N*-acetyl groups (N-Ac) abolished the HS-Tie1 interaction. Removal of the *N*-sulfate groups (De-N) or the 2-O-sulfate groups (De-2O) greatly reduced HS-Tie1 binding. Data represent mean  $\pm$  s.e.m.; n=2 independent replicates.



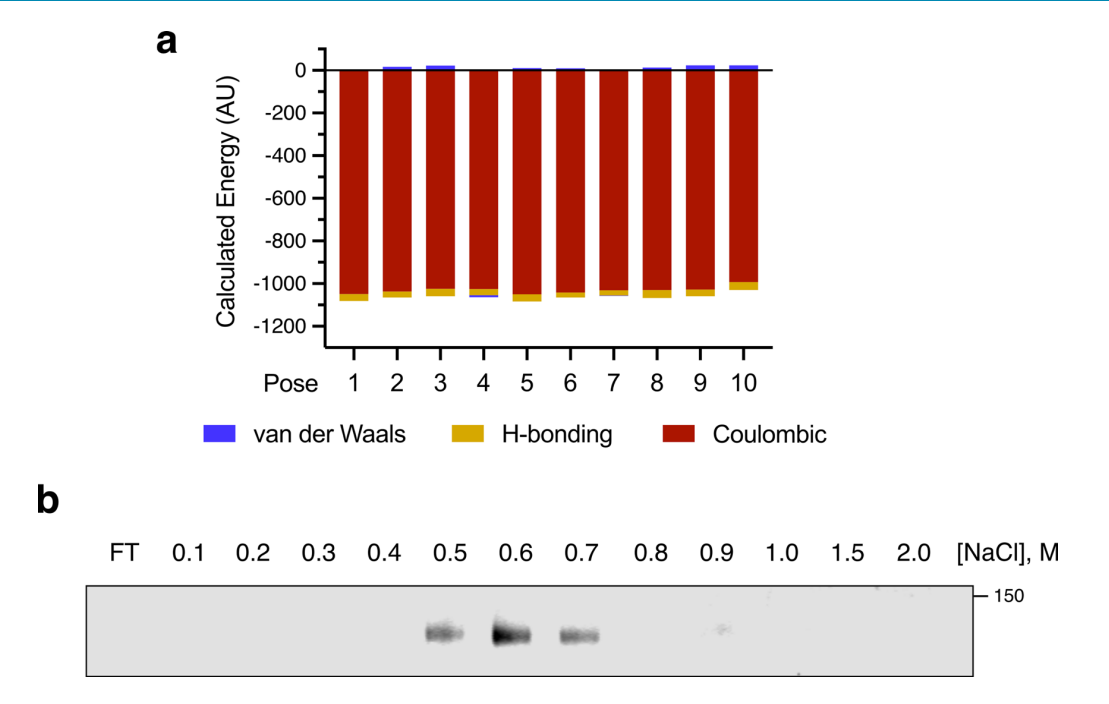
**Extended Data Fig. 4 | Soluble Tie1 binds to HUVECs.** Immunofluorescence imaging and orthogonal plane views of HUVECs with cell-associated Tie1-Fc (yellow), scale bar =  $5 \,\mu$ m. Red bars indicate cross-sectional views in xz and yz images, which were produced by combining z-stack images using FIJI/ImageJ. The majority of Tie1 appears at the apical or basolateral cell surface. Representative images from four individual cells are shown.



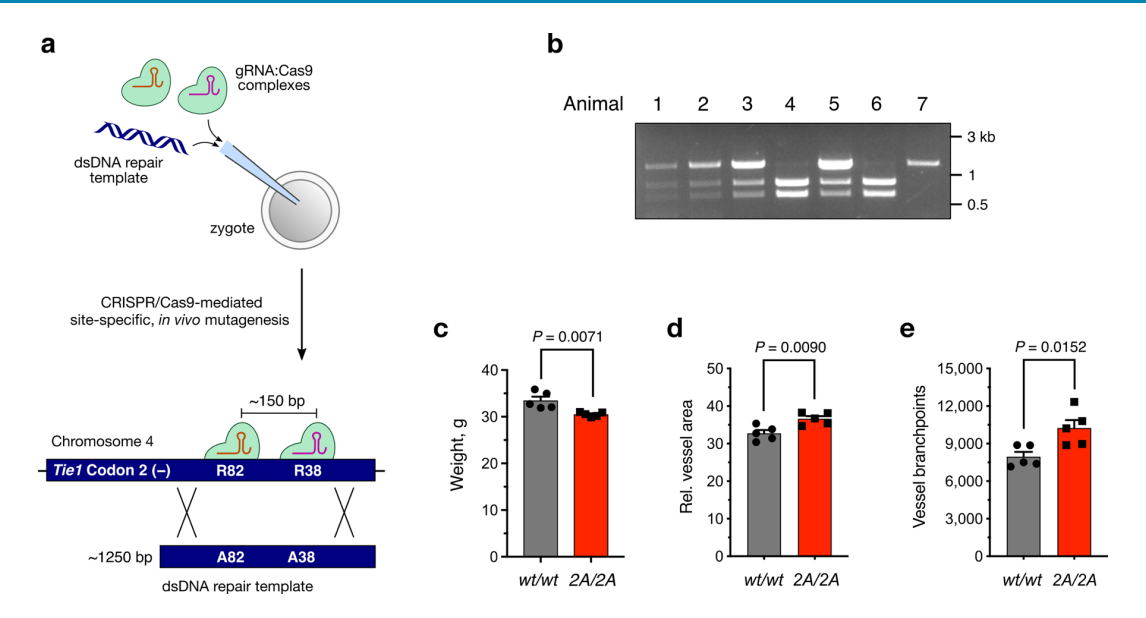
**Extended Data Fig. 5 | Sulfated HS GAGs engage Tie1 in its N-terminal domains. a** Schematic and **b** Western blot of overexpressed, purified full-length (Tie1-FL) and C-terminal truncated (Tie-N) Tie1 ectodomains. Colors in (a) correspond to the ribbon diagram of Tie1 in Fig. 4a. Gray sections are derived from the expression plasmid. **c**, Binding of biotinylated triS-HS to recombinant Tie1-FL and Tie-N by ELISA. Data for (c) were obtained in the same experiment as Fig. 4e. Dissociation constants, as determined by ELISA:  $K_{D,app}$  (Tie1-FL) = 6.51nM (5.58 to 7.63 nM),  $K_{D,app}$  (Tie1-N) = 6.26 nM (5.26 to 7.45 nM); values represent mean (95% CI); graphed data represent n=2 independent replicates.



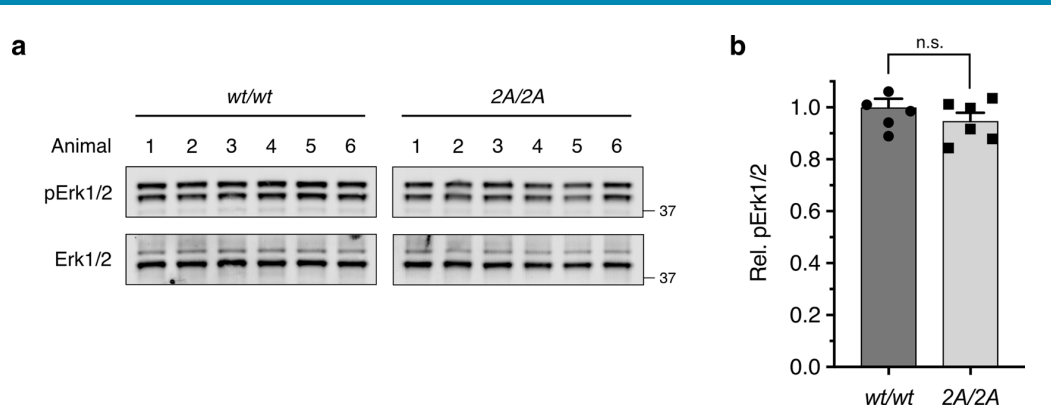
**Extended Data Fig. 6 | HS GAGs** engage Tie1 in an electropositive region of the first N-terminal Ig-like domain. a Ribbon diagram and **b** electrostatic potential surface of the Tie2 crystal structure (pdb 2GY5), which lacks the electropositive HS binding site found in Tie1. The red to blue scale in (b) represents relative electrostatic potential (electronegative to electropositive). **c**, Schematic of the first N-terminal Ig-like domain (Ig1) of Tie1, highlighting the six positively charged amino acids within 5-10 Å of the top 10 highest ranked HS GAG docked poses. All residues are mutated to alanine in the Tie1-6A construct, whereas only the two bolded residues are mutated in Tie1-2A. **d**, Structural model of the Tie1 N-terminal region (residues 22-447) indicating key amino acid residues involved in HS binding (purple) and those reported to be involved in Tie2 binding (orange)<sup>27</sup>. Distances are displayed in angstroms between the alpha carbon of each residue. **e**, Western blot showing expression of secreted Tie1 ectodomain constructs from HEK-293T cells after purification.



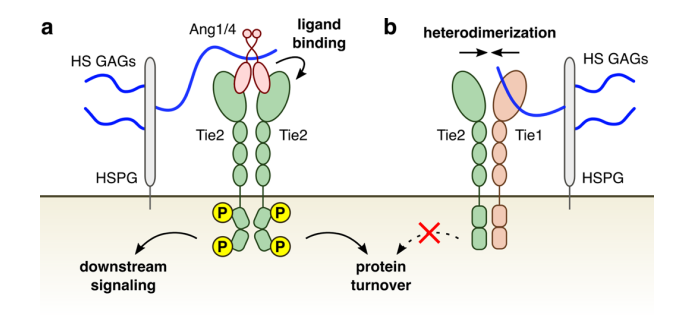
**Extended Data Fig. 7 | The HS-Tie1 interaction is driven primarily by ionic interactions. a**, Relative energetic contributions of van der Waals, hydrogen bonding, and Coulombic forces to the total calculated nonbonding energy are shown for the top 10 HS-Tie1 binding poses. In all cases, Coulombic forces dominated the calculated energy. **b**, Salt elution profile of Tie1 bound to heparin-sepharose shows loss of the HS-Tie1 interaction with increasing NaCl concentrations, indicative of strong ionic interactions between HS and Tie1. FT = flow-through.



**Extended Data Fig. 8** | Generation, genotyping, and characterization of Tie1-2A mice. **a**, Schematic of the homology-directed repair method used to generate the Tie1-2A mouse line incorporating R38A and R82 A mutations into the endogenous murine *Tie1* gene. **b**, Representative genotyping results from a *Tie1*<sup>2A/wt</sup> x *Tie1*<sup>2A/wt</sup> breeding pair after the Tie1 locus was amplified by PCR and digested with Stul. Animal 7 is  $Tie1^{wt/wt}$ , animals 1, 2, 3, and 5 are  $Tie1^{2A/wt}$ , and animals 4 and 6 are  $Tie1^{2A/2A}$ . **c**, Quantification of weight differences between  $Tie1^{2A/2A}$  (2A/2A) and wild-type (wt/wt) 4-month-old, male littermates, n=5 per genotype. **d**,**e**, Quantification of relative vessel area and branchpoints from retinal samples described in Fig. 6; n=5 per genotype. Data represent mean  $\pm$  s.e.m.; unpaired, two-tailed Student's t test.



**Extended Data Fig. 9** | **Tie1 mutation does not affect Erk1/2 phosphorylation** *invivo.* **a**, Representative Western blots and **b**, quantification of pErk1/2 from lung tissue harvested from 7-day-old pups; n = 6 per genotype. pErk1/2 values were normalized to the corresponding total Erk1/2 levels and are reported relative to the wild-type animals. All gels were transferred to the same blot and imaged to allow for direct comparison between samples. Data represent mean  $\pm$  s.e.m.; unpaired, two-tailed Student's t test.



**Extended Data Fig. 10 | HS GAGs regulate the Ang/Tie signaling pathway.** HS GAGs utilize two distinct binding modes to promote pathway activation. **a**, Endothelial cell-associated HS GAGs recruit agonistic ligands Ang1 and Ang4 to form HS-Ang-Tie2 complexes and elicit downstream signaling. **b**, HS GAGs also bind to the orphan receptor Tie1 to promote the Tie1-Tie2 interaction, which maintains Tie2 protein levels and prevents protein turnover at the cell surface to sustain downstream signaling.

## natureresearch

Corresponding author(s): Linda C. Hsieh-Wilson

Last updated by author(s): 7/29/2020

### **Reporting Summary**

Nature Research wishes to improve the reproducibility of the work that we publish. This form provides structure for consistency and transparency in reporting. For further information on Nature Research policies, see Authors & Referees and the Editorial Policy Checklist.

| _  |     |   |     |     |
|----|-----|---|-----|-----|
| ζ. | ta: | t | ıst | ics |

| For         | all st      | atistical analyses, confirm that the following items are present in the figure legend, table legend, main text, or Methods section.   |
|-------------|-------------|---|
| n/a         | Cor         | nfirmed   |
|             | $\boxtimes$ | The exact sample size $(n)$ for each experimental group/condition, given as a discrete number and unit of measurement   |
|             | $\boxtimes$ | A statement on whether measurements were taken from distinct samples or whether the same sample was measured repeatedly   |
|             | $\boxtimes$ | The statistical test(s) used AND whether they are one- or two-sided Only common tests should be described solely by name; describe more complex techniques in the Methods section.  |
| X           |             | A description of all covariates tested  |
|             | $\boxtimes$ | A description of any assumptions or corrections, such as tests of normality and adjustment for multiple comparisons   |
|             | $\boxtimes$ | A full description of the statistical parameters including central tendency (e.g. means) or other basic estimates (e.g. regression coefficient AND variation (e.g. standard deviation) or associated estimates of uncertainty (e.g. confidence intervals) |
|             | $\boxtimes$ | For null hypothesis testing, the test statistic (e.g. <i>F</i> , <i>t</i> , <i>r</i> ) with confidence intervals, effect sizes, degrees of freedom and <i>P</i> value noted <i>Give P values as exact values whenever suitable.</i>                       |
| $\times$    |             | For Bayesian analysis, information on the choice of priors and Markov chain Monte Carlo settings  |
| $\boxtimes$ |             | For hierarchical and complex designs, identification of the appropriate level for tests and full reporting of outcomes  |
| $\times$    |             | Estimates of effect sizes (e.g. Cohen's $d$ , Pearson's $r$ ), indicating how they were calculated  |
|             |             | Our web collection on <u>statistics for biologists</u> contains articles on many of the points above.   |

#### Software and code

Policy information about availability of computer code

Data collection

All instrument-generated data were collected using the manufacturer's associated software as described in the Online Methods. Plate reader data were collected by SoftMax Pro (Ver. 5, Molecular Devices). Microarray data were collected by GenePix (Ver. 5.0, Molecular Devices). SPR data were collected by Biacore T200 Evaluation Software (Ver. 1, GE Healthcare). Cell and tissue images were collected by ZEN Software (Ver. 8.1, Carl Zeiss). Gel images were collected by ImageStudio (Ver. 5.2.5, LI-COR Biosciences).

Data analysis

Computational docking studies were conducted using methods and software from a previously described publication (Griffith AR et al. Proc. Natl. Acad. Sci. U.S.A. 114 (2017), 13697-13702). Software associated with this procedure includes SWISS-MODEL for homology model generation (accessed May 2016, https://swissmodel.expasy.org/), DREIDING for minimalization (in house, Ver. May 2016), MPsim for molecular dynamics (in house, Ver. May 2016), and SCREAM for side chain optimization (in house, Ver. May 2016). Imaging data were analyzed using Fiji/ImageJ (Ver. 2.0.0-rc-43/1.51w, NIH). Immunoblotting data were analyzed by ImageStudio (Ver. 5.2.5, LI-COR Biosciences). Guide RNAs were designed by CHOPCHOP (Ver. 2, https://chopchop.cbu.uib.no/). All statistical analyses were conducted by Prism 7 for Mac (Ver. 7.0d, Graphpad) and Microsoft Excel for Mac (Ver. 16.16.2).

For manuscripts utilizing custom algorithms or software that are central to the research but not yet described in published literature, software must be made available to editors/reviewers. We strongly encourage code deposition in a community repository (e.g., GitHub). See the Nature Research guidelines for submitting code & software for further information.

#### Data

Policy information about availability of data

All manuscripts must include a data availability statement. This statement should provide the following information, where applicable:

- Accession codes, unique identifiers, or web links for publicly available datasets
- A list of figures that have associated raw data
- A description of any restrictions on data availability

Any data generated or analyzed during this study are included in the article and related supplemental information or are available from the corresponding author

|  | est. Publicly available data used in this study include the Tie2 crystal structure (PDB ID 2GY5), the Tie1 protein sequence (UniProt ID P335590), e genome assembly (GRCm38/mm10), and the CHOPCHOP guide RNA design tool (https://chopchop.cbu.uib.no/).   |  |  |  |  |
|--|---|--|--|--|--|
| Field-spe  | ecific reporting  |  |  |  |  |
| Please select the o                                  | ne below that is the best fit for your research. If you are not sure, read the appropriate sections before making your selection.   |  |  |  |  |
| ∠ Life sciences                                      | Behavioural & social sciences Ecological, evolutionary & environmental sciences   |  |  |  |  |
| For a reference copy of                              | the document with all sections, see <u>nature.com/documents/nr-reporting-summary-flat.pdf</u>   |  |  |  |  |
|  |   |  |  |  |  |
| Life scier   | nces study design   |  |  |  |  |
| All studies must dis                                 | close on these points even when the disclosure is negative.   |  |  |  |  |
| Sample size  | No statistical analyses were used to predetermine sample size. Sample sizes for all experiments were chosen based on previous publications from our laboratory (Shipp EL, Hsieh-Wilson LC. Chem. Biol. 14 (2007), 195-208; Brown JM et al. Proc. Natl. Acad. Sci. U.S.A. 109 (2012), 4768-4773; Pulsipher A et al. Angew. Chem. Int. Ed. 54 (2015), 1466-1470) and others (Savant S et al. Cell Rep. 12 (2015): 1761-1773; Korhonen EA et al. J. Clin. Invest. 126 (2016), 3495-3510; Xu D et al. J. Biol. Chem. 286 (2015): 737-745) as cited in the text to account for intrinsic variability of the experiments. |  |  |  |  |
| Data exclusions                                      | No data were excluded from analyses.  |  |  |  |  |
| Replication  | All cell-based assays were successfully replicated as independent experiments described in the text and supporting information. All animal tissue-based assays were performed using samples acquired from litter mates from at least two biologically independent litters that were processed and analyzed together after genotyping.   |  |  |  |  |
| Randomization  | No randomization was applied in these experiments. Specific controls for covariates in the protein- and cell-based assays were not relevant as identical protocols and reagents were used within each assay across all samples except for the variable being tested. Animals were allocated based on genotype, and age-matched litter mates were used to minimize covariance in the biological source material.   |  |  |  |  |
| Blinding   | No blinding was applied in these experiments. All data acquisition and analysis were performed automatically where possible by software described above and in the text and supporting information. For the FoxP3 nuclear export assay, the FoxP3 fluorescence signal of the costained nucleus and adjacent cytosol of each cell in a field of view was measured by software, and the categorical, binary assignment of FoxP3 nuclear status of each cell was conducted by a single, unblinded investigator based on this quantitative data to prevent investigator bias.   |  |  |  |  |
| We require informati                                 | g for specific materials, systems and methods on from authors about some types of materials, experimental systems and methods used in many studies. Here, indicate whether each material, ted is relevant to your study. If you are not sure if a list item applies to your research, read the appropriate section before selecting a response.   |  |  |  |  |
| Materials & ex                                       | perimental systems Methods  |  |  |  |  |
| n/a Involved in the study  n/a Involved in the study |   |  |  |  |  |
| Antibodies   | ChIP-seq  |  |  |  |  |
| Eukaryotic   | Eukaryotic cell lines Flow cytometry  |  |  |  |  |
|  | Palaeontology MRI-based neuroimaging  |  |  |  |  |
| -1-  | Animals and other organisms   |  |  |  |  |
| Human res  | Human research participants   |  |  |  |  |

#### **Antibodies**

Antibodies used

Clinical data

Antibodies used in the manuscript as are follows: Rb anti-His-tag (Cell Signaling Technology, 12698S, D3I10); Gt anti-Tie1 (R&D Systems, AF619); Rb anti-Tie1 (Cell Signaling Technology, 23111S); Ms anti-Tie1 (R&D Systems, MAB619); Rb anti-phospho-Tie2 (R&D Systems, AF2720); Gt anti-Tie2 (R&D Systems, AF313); Gt anti-Tie2 (R&D Systems, AF762); Rb anti-Tie2 (Santa Cruz Biotechnology, H176); Rb anti-phospho-Akt (Cell Signaling Technology, 9275S); Ms anti-Akt (Cell Signaling Technology, 2920S, 40D4); Ms anti-alpha-tubulin (MilliporeSigma, T9026, DM1A); Rb anti-phospho-p44/42 MAPK (or Erk1/2) (Cell Signaling Technology, 9101S); Ms anti-p44/42 MAPK (or Erk1/2) (Cell Signaling Technology, 4696S, L34F12); Rb anti-FOXO1 (Cell Signaling Technology, 2880S, C29H4); Ms anti-HS (370255-S, Amsbio, F58-10E4); Gt anti-Ms Alexa Fluor 488 (ThermoFisher, A11001); Gt anti-Ms Alexa Fluor 680 (ThermoFisher, A21057); Gt anti-Ms Alexa Fluor 790 (ThermoFisher, A11357), Gt anti-Rb Alexa Fluor 568 (ThermoFisher, A11036), Gt anti-Rb Alexa Fluor 680 (ThermoFisher, A21076), Gt anti-Rb Alexa Fluor 790 (ThermoFisher, A11369), Dk anti-Gt Alexa Fluor 680 (ThermoFisher, A32860), Gt anti-Hm Fc Alexa Fluor 647 (Jackson ImmunoResearch, 109-605-098). Specific lot numbers are unavailable.

#### Validation

All antibodies were commercially available and used for applications previously validated by the manufacturers and in relevant citations on the manufacturers' websites or in house.

Rb anti-His-tag (Cell Signaling Technology, 12698S, D3I10): Manufacturer validated Western blotting against recombinant

Gt anti-Tie1 (R&D Systems, AF619): Manufacturer validated Western blotting using recombinant Tie1.

Rb anti-Tie1 (Cell Signaling Technology, 23111S): Manufacturer validated for Western blotting with expressing cell lines. Ms anti-Tie1 (R&D Systems, MAB619): Manufacturer validated for cell imaging and Western blotting using cell lines and recombinant Tie1, respectively.

Rb anti-phospho-Tie2 (R&D Systems, AF2720): Manufacturer validated for Western blotting using stimulated cell lines. Gt anti-Tie2 (R&D Systems, AF313): Manufacturer validated for Western blotted using cell lines.

Gt anti-Tie2 (R&D Systems, AF762): Manufacturer validated for Western blotting using recombinant protein.

Rb anti-Tie2 (Santa Cruz Biotechnology, H176): Manufacturer validated for cell staining using cell lines.

Rb anti-phospho-Akt (Cell Signaling Technology, 9275S): Manufacturer validated for Western blotting using stimulated cell lines.

Ms anti-Akt (Cell Signaling Technology, 2920S, 40D4): Manufacturer validated for Western blotting using cell lines. Ms anti-alpha-tubulin (MilliporeSigma, T9026, DM1A): Manufacturer validated for Western blotting using cell lines.

Rb anti-phospho-p44/42 MAPK (or Erk1/2) (Cell Signaling Technology, 9101S): Manufacturer validated for Western blotting using

Ms anti-p44/42 MAPK (or Erk1/2) (Cell Signaling Technology, 4696S, L34F12): Manufacturer validated for Western blotting using cell lines.

Rb anti-FOXO1 (Cell Signaling Technology, 2880S, C29H4): Manufacturer validated for cell imaging using stimulated cell lines. Ms anti-HS (370255-S, Amsbio, F58-10E4): Manufacturer validated for cell imaging using knockout cell lines.

Gt anti-Ms Alexa Fluor 488 (ThermoFisher, A11001): Manufacturer validated for cell imaging detection using Ms IgG

Gt anti-Ms Alexa Fluor 680 (ThermoFisher, A21057): Manufacturer validated for Western secondary detection using Ms IgG.

Gt anti-Ms Alexa Fluor 790 (ThermoFisher, A11357): Manufacturer validated for Western secondary detection using Ms IgG.

Gt anti-Rb Alexa Fluor 568 (ThermoFisher, A11036): Manufacturer validated for cell imaging detection using Rb IgG. Gt anti-Rb Alexa Fluor 680 (ThermoFisher, A21076): Manufacturer validated for Western secondary detection using Rb IgG.

Gt anti-Rb Alexa Fluor 790 (ThermoFisher, A11369): Manufacturer validated for Western secondary detection using Rb IgG.

Dk anti-Gt Alexa Fluor 680 (ThermoFisher, A32860): Manufacturer validated for Western secondary detection using Gt IgG. Gt anti-Hm Fc Alexa Fluor 647 (Jackson ImmunoResearch, 109-605-098): Manufacturer validated for Hm Fc specificity by ELISA and was also co-validated for specificity on microarrays in house with similar results to other Gt anti-Hm Fc secondary antibodies used previously (Brown JM et al. Proc. Natl. Acad. Sci. U.S.A. 109 (2012): 4768-4773).

#### Eukaryotic cell lines

Policy information about cell lines

Cell line source(s)

HEK-293T (ATCC CRL-3216), EA.hy926 (ATCC CRL-2922), and HUVEC, pooled (ATCC PCS-100-013)

Authentication

Cells were used as received from ATCC without further authentication.

Mycoplasma contamination

Cells were used as received from ATCC without further testing for mycoplasma contamination. No nonnuclear puncta were observed from DAPI staining during immunofluorescence experiments.

Commonly misidentified lines (See ICLAC register)

The study did not use any commonly misidentified cell lines.

#### Animals and other organisms

Policy information about studies involving animals; ARRIVE guidelines recommended for reporting animal research

Laboratory animals

The Tie1-2A mouse line was generated using B6SJL-F1/J founders (Jackson Laboratory) and backcrossed with C57BL/6J mice (Jackson Laboratory) as described in the Online Methods. Animals were maintained with no more than five adult animals per cage in small mouse cages with enrichment under 20-26C ambient temperature, 30-70% relative humidity, and a 12-h light-dark cycle. General animal maintenance and timed matings were performed by members of the Caltech Office of Laboratory Animal Resources with cage changes performed weekly. For retinal tissue harvesting, litter mates of both sexes at P7 were used. For lung tissue harvesting, litter mates of both sexes at 4 months of age were used.

Wild animals

The study did not involve wild animals.

Field-collected samples

The study did not involve field-collected samples.

Ethics oversight

All procedures involving animals were approved by the Caltech Institutional Animal Care and Use Committee prior to the start of all experiments.

Note that full information on the approval of the study protocol must also be provided in the manuscript.